


Review

Open Access



# Nanoarchitectonics and applications of two-dimensional materials as anodes for lithium-ion capacitors

Tao Hu<sup>1,2</sup>, Xiong Zhang<sup>1,2,3,\*</sup> , Yabin An<sup>1,2,3</sup>, Shasha Zhao<sup>1,2</sup>, Chen Li<sup>1,3,\*</sup>, Xianzhong Sun<sup>1,2,3</sup>, Kai Wang<sup>1,2,3</sup>, Yanwei Ma<sup>1,2,3,\*</sup>

<sup>1</sup>Institute of Electrical Engineering, Chinese Academy of Sciences, Beijing 100190, China.

<sup>2</sup>School of Engineering Sciences, University of Chinese Academy of Sciences, Beijing 100049, China.

<sup>3</sup>Shandong Key Laboratory of Advanced Electromagnetic Conversion Technology, Institute of Electrical Engineering and Advanced Electromagnetic Drive Technology, Qilu Zhongke, Jinan 250013, Shandong, China.

\*Correspondence to: Prof. Xiong Zhang, Institute of Electrical Engineering, Chinese Academy of Sciences, No. 6 Beiertiao, Zhongguancun, Beijing 100190, China. E-mail: zhangxiong@mail.iee.ac.cn; Prof. Chen Li, Institute of Electrical Engineering, Chinese Academy of Sciences, No. 6 Beiertiao, Zhongguancun, Beijing 100190, China. E-mail: lichen@mail.iee.ac.cn; Prof. Yanwei Ma, Institute of Electrical Engineering, Chinese Academy of Sciences, No. 6 Beiertiao, Zhongguancun, Beijing 100190, China. E-mail: ywma@mail.iee.ac.cn

**How to cite this article:** Hu T, Zhang X, An Y, Zhao S, Li C, Sun X, Wang K, Ma Y. Nanoarchitectonics and applications of two-dimensional materials as anodes for lithium-ion capacitors. *Energy Mater* 2025;5:500003. <https://dx.doi.org/10.20517/energymater.2024.43>

**Received:** 8 May 2024 **First Decision:** 21 Jun 2024 **Revised:** 3 Jul 2024 **Accepted:** 17 Jul 2024 **Published:** 30 Jul 2024

**Academic Editor:** Liming Jin **Copy Editor:** Fangling Lan **Production Editor:** Fangling Lan

## Abstract

Lithium-ion capacitors (LICs) represent an innovative hybridization in the energy storage field, effectively combining the best features of supercapacitors and lithium-ion batteries. However, the theoretical advantage of LICs is impeded by the low reaction efficiency of the negative electrode material and significant volume expansion. Two-dimensional (2D) materials, due to their unique morphology, abundant pores, rich active centers, and adjustable composition, have been widely studied and developed as negative electrodes for LICs. Therefore, it is imperative to provide a timely review of the latest advancements in the field. The review initiates with a detailed exploration of the infrastructure, key performance evaluation parameters, and the underlying energy storage mechanisms that define LICs. Subsequently, the focus shifts towards the cutting-edge research surrounding 2D materials, including graphene, MXene, transition-metal dichalcogenides, and transition-metal oxides. The review further elaborates on the typical applications of these 2D materials within LIC frameworks, highlighting their unique properties and contributions to enhanced energy storage solutions. In conclusion, the discussion addresses the significant challenges these materials encounter within LIC applications, such as scalability, cost, and integration



© The Author(s) 2024. **Open Access** This article is licensed under a Creative Commons Attribution 4.0 International License (<https://creativecommons.org/licenses/by/4.0/>), which permits unrestricted use, sharing, adaptation, distribution and reproduction in any medium or format, for any purpose, even commercially, as long as you give appropriate credit to the original author(s) and the source, provide a link to the Creative Commons license, and indicate if changes were made.



issues, while also projecting future development prospects. It outlines both the current limitations and the potential breakthroughs that could pave the way for more advanced and efficient LIC technologies.

**Keywords:** Two-dimensional anode materials, MXene, graphene, transition-metal dichalcogenides, transition-metal oxides, lithium-ion capacitors

## INTRODUCTION

Climate change and environmental concerns have garnered increasing global attention. Scientific research underscores human-induced greenhouse gas emissions as a key driver of climate change, with adverse effects including environmental pollution and resource overconsumption, profoundly affecting both society and ecosystems<sup>[1-4]</sup>. To address these challenges, nations worldwide are implementing measures to enhance energy efficiency and reduce emissions, reflecting a global consensus on the imperative of energy security and sustainable development. Simultaneously, recognizing the risks posed by fossil fuel dependence, countries are transitioning towards cleaner, renewable energy sources, expediting structural adjustments in energy systems to foster diversified and sustainable energy provision<sup>[5-7]</sup>. With the remarkable growth in the annual generation of wind and solar energy and the rapid growth of modern energy storage demand, there is an immediate need to create energy storage solutions characterized by substantial energy capacity, formidable power capabilities, and extended operational lifespans<sup>[8-10]</sup>. Over the past few decades, two promising candidates, lithium-ion batteries (LIBs) and supercapacitors (SCs), have stood out and have been widely applied in a variety of energy storage fields<sup>[11-15]</sup>. LIBs are distinguished by their impressive energy density (ED), which typically ranges from 150 to 300 Wh·kg<sup>-1</sup>. This high ED allows LIBs to store a substantial amount of energy relative to their mass, making them particularly advantageous for applications where long-term energy storage is critical<sup>[16-18]</sup>, and SCs are renowned for their exceptionally high power density (PD), which can exceed 10 kW·kg<sup>-1</sup>, coupled with their remarkable cycling stability, enduring anywhere from 10<sup>4</sup> to 10<sup>5</sup> charge-discharge cycles. These characteristics render SCs especially suitable for scenarios that demand rapid energy delivery and robust cycle endurance<sup>[19-24]</sup>. However, with the continuous development of energy technology, the lower PD (< 1 kW·kg<sup>-1</sup>) of LIBs and the lower ED (5-10 Wh·kg<sup>-1</sup>) of SCs are insufficient to meet the developing energy storage needs<sup>[25-27]</sup>.

In 2001, Amatucci *et al.* first achieved a significant breakthrough by fabricating a LIC [Figure 1A] through the combination of LIBs-type anode (Li<sub>4</sub>Ti<sub>5</sub>O<sub>12</sub>, LTO) and SCs-type cathode (activated carbon, AC)<sup>[28,29]</sup>. These LICs showcased an upper ED (> 20 Wh·kg<sup>-1</sup>), while simultaneously keeping a superior cycle lifespan (> 5,000 cycles) and an impressive ability to handle high discharge rates (with a 90% capacity retention even under a high discharge rate of 10C), which demonstrated that LICs offer an effective means of striking a balance [Figure 1B] between LIBs and SCs<sup>[30]</sup>. To date, various LICs have been reported and extensively studied<sup>[31-37]</sup>. For instance, the ED and PD of LICs are profoundly influenced by the electrode materials, which include the operation potential range, specific capacity, rate capability, and cycle life<sup>[38-47]</sup>. Recognizing this, researchers are dedicating significant efforts towards developing advanced electrode materials that can enhance the overall functionality of LICs. Currently, the electrode materials used in LICs are often adapted from those originally developed for LIBs and SCs. Specifically, carbon materials, typical SCs-type materials, are employed in LICs due to their high specific surface area (SSA) and robust cycle stability which are crucial for long-term performance and excellent conductivity<sup>[48-58]</sup>. However, the adaptation of LIBs-type materials into LICs has encountered several challenges. These materials often suffer from low PD, unbalanced charge-discharge rates, poor conductivity, and significant volume changes during operation, which can severely undermine the efficiency and lifespan of LICs<sup>[59]</sup>. Therefore, there is a pressing need for ideal LIBs-type electrode materials that feature short charge storage paths, limited volume expansion during operation, high conductivity and relatively low operating potentials to effectively address these issues<sup>[60-62]</sup>.

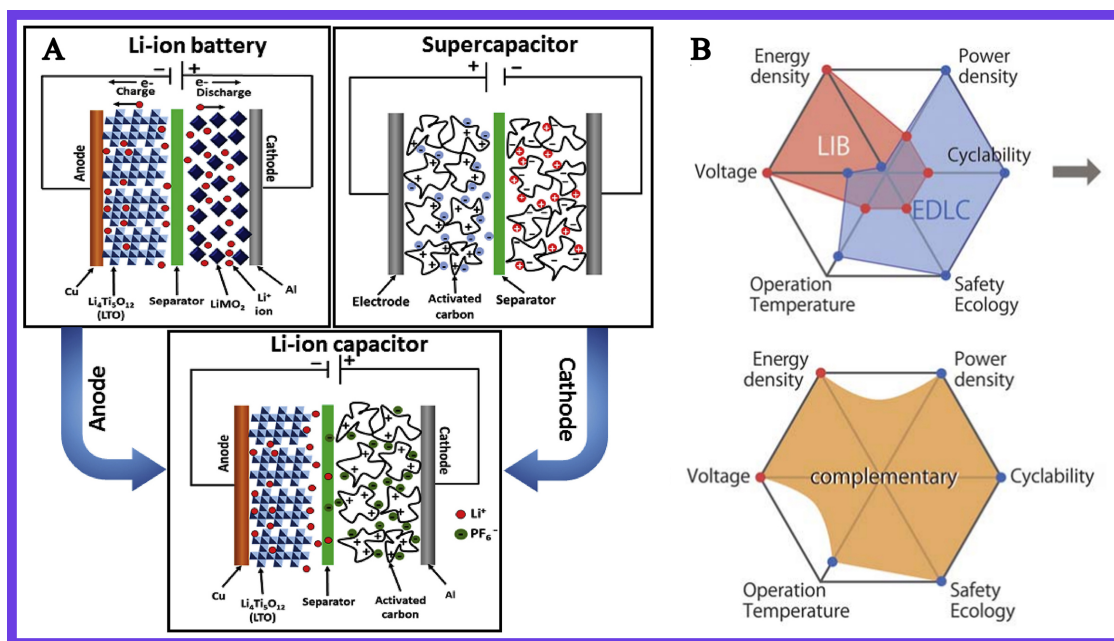


**Figure 1.** (A) Construction of LICs. Reproduced with permission<sup>[29]</sup>. Copyright 2019, Elsevier B.V.; (B) The relationship and comparison between LICs, LIBs and SCs. Reproduced with permission<sup>[30]</sup>. Copyright 2012, The Royal Society of Chemistry.

Since the discovery of graphene, a thin sheet composed of a monolayer of carbon atoms, by Novoselov and Geim in 2004<sup>[63]</sup>, this type of material has attracted widespread attention in many fields, particularly in energy storage and conversion<sup>[64-68]</sup>. Two-dimensional (2D) materials commonly consist of only two atomic layers or planes, typically measuring only a few atoms or molecules in thickness. As a result, they exhibit remarkably thinner structures than their multilayer bulk materials, which imparts various superb properties, including large surface area<sup>[69,70]</sup>, impressive mechanical adaptability<sup>[71]</sup>, adjustable electronic properties<sup>[72,73]</sup>, and heightened electrochemical reactivity<sup>[74,75]</sup>. Therefore, when applied to the negative electrode of LICs, they always show excellent electrochemical properties<sup>[76-78]</sup>:

- High capacitive performance: the substantial surface area of 2D materials provides numerous active sites and can shorten lithium-ion ( $\text{Li}^+$ ) transport pathways.
- Long cycle life: based on the structural stability of 2D materials, they typically boast an extended cycle life, enduring thousands of charge and discharge cycles without failure.
- Excellent electrical conductivity: 2D materials often exhibit exceptional electrical conductivity, contributing to the enhancement of PD and charging speed in LICs.

Nevertheless, challenges still persist in the pursuit of fast  $\text{Li}^+$  insertion/de-insertion for 2D anode materials. These challenges include understanding the energy storage mechanisms of original 2D anode materials, navigating fussy synthesis methods, and addressing the stability of multi-stage structures necessitated by the demands of the structure-property relationship. Overcoming these hurdles is essential for unlocking the full performance of 2D anode materials in advanced energy storage applications.

Currently, 2D materials have become a promising potential anode<sup>[79]</sup>. The review specifically emphasizes the potential of 2D materials, providing a concentrated examination of their unique properties and advantages, including graphene, transition-metal oxides (TMOs), transition-metal dichalcogenides (TMDs), and MXenes, offering a comprehensive overview rather than focusing on a single type of material. Additionally, the review details specific strategies to enhance capacitive charge storage, such as doping<sup>[80,81]</sup>, tuning of pore structures<sup>[82]</sup>, reduction of nanosheet thickness<sup>[83,84]</sup>, expansion of inter-layer spacings<sup>[85-88]</sup>, and the construction of hybrid heterostructures<sup>[86,89-92]</sup>. By focusing on the reduction of contact path lengths to surface active sites and impedance to Li<sup>+</sup> intercalation, the review provides a thorough investigation of how these aforementioned strategies improve performance.

## A BRIEF INTRODUCTION OF LICs

### Basic configuration

LICs integrate material characteristics of both SCs and LIBs, encompassing an electrolyte and a separator within their architecture [Figure 1A]. The potential of LICs is deeply influenced by the selection of electrode materials, their relative proportions, and their structural arrangement. For instance, due to its extensive SSA and favorable conductivity, AC is predominantly used as the cathode, which are essential for the rapid ion adsorption/desorption process. In contrast, the role of the negative electrode is pivotal in defining the PD of LICs, primarily because it involves the slower reaction kinetics associated with the Li<sup>+</sup> insertion/extraction, unlike the more rapid processes occurring at the positive electrode. Consequently, the choice of material for the negative electrode becomes crucial due to its significant influence on the kinetics of reactions and, by extension, the overall PD of the capacitor. Although LICs generally employ standard battery components for their electrolytes and separators, these are not the primary focus of current research discussions. This review underscores the importance of material selection and structural design in LICs, particularly highlighting the critical roles played by the negative electrodes in optimizing the functionality and efficiency of these devices.

### Performance evaluation parameter

ED and PD serve as fundamental metrics for evaluating the performance of LICs. The determination of these parameters is typically achieved by integrating the area under the constant current discharge curve, utilizing specific equations that accommodate both linear and non-linear galvanostatic charge/discharge (GCD) curves, as expressed by:

$$E = \int U dQ = \int_{t_1}^{t_2} U I dt \quad (1)$$

$$P = E/t \quad (2)$$

According to these equations, the overall performance of LICs is predominantly influenced by two critical factors: the operating voltage (U) of the device and the capacity (Q) of the electrode materials. Currently, the operating voltage range for commercial LICs spans from 2.2 to 3.8 volts, which is slightly less than the maximum voltage limit of 4.45 volts attainable by LIBs<sup>[93,94]</sup>. To improve both the ED and PD of LICs, it is urgent to extend the operating voltage window and to develop electrode materials that not only possess high capacity but also exhibit high-rate performance and robust structural stability.

### Energy storage mechanism

The difference in electrochemical performance is mainly attributed to a rich diversity of active materials, each offering unique properties and functionalities essential for various applications. These materials are primarily classified according to their structural dimensions and reaction mechanisms. Structurally, they range from zero-dimensional forms such as nanoparticles and quantum dots, which are tiny and capable of



high surface reactions, to one-dimensional forms including nanowires, nanotubes, and nanobelts that provide directional conductivity and mechanical strength. Additionally, 2D materials such as nanosheets offer extensive surface areas and unique electronic properties, while three-dimensional (3D) structures encompass nanoporous frameworks that are ideal for facilitating bulk ion transport and storage.

In terms of reaction mechanisms, these materials can be categorized into those that operate through surface ion adsorption, which involves the ion accumulation on the surface of the materials, and those that facilitate fast redox reactions via ion intercalation, allowing for quick charge and discharge cycles. Additionally, some materials exhibit pseudo-capacitive properties, where charge is stored by means of electrochemical reactions on or near the surface, leading to high power densities. Based on the device construction, LICs can be broadly divided into three categories [Figure 2]:

(1) LIBs-type negative electrode//SCs-type positive electrode [Figure 2A]:

This configuration of LICs is currently the most common and encompasses the widest range of material types. The negative electrode comprises LIBs-type materials, including embeddable graphite, soft carbon, LTO, or  $\text{Li}_3\text{VO}_4$ , as well as conversion-type metal oxides (such as MnO, CoO, and NiO) and alloying reactions of Si, Se, and Sn. The positive electrode consists of capacitive porous carbon materials, generally commercial AC, among which an all-carbon-type LIC (e.g., AC//graphite) is the most classic configuration. During charging process,  $\text{Li}^+$  from the electrolyte are embedded into the LIBs-type negative electrode material, while the surface of the positive electrode adsorbs anions, thus achieving charge balance across the entire system. Throughout the process, ions in the electrolyte primarily play the role of storing and releasing energy; hence, it can also be termed the electrolyte consumption mechanism.

(2) SCs-type negative electrode//LIBs-type positive electrode [Figure 2B]:

In this system, common LIBs-type positive electrode materials such as  $\text{LiMn}_2\text{O}_4$  and  $\text{LiFePO}_4$  are utilized. When charging,  $\text{Li}^+$  are released from the material into the electrolyte. Simultaneously, the SCs-type material on the negative electrode side (such as AC) adsorbs  $\text{Li}^+$  from the electrolyte. The entire process is reversible and does not consume  $\text{Li}^+$  from the electrolyte. Similar to the operation of LIBs, thus, it can be considered as a  $\text{Li}^+$  transport mechanism overall.

(3) LIBs-type negative electrode//LIBs-type composite SCs-type positive electrode [Figure 2C]:

The positive electrode material of this type of LIC configuration is typically composed of a combination of materials utilizing two energy storage mechanisms, such as  $\text{AC} + \text{LiMn}_2\text{O}_4$ ,  $\text{AC} + \text{LiCoO}_2$ , or  $\text{AC} + \text{LiFePO}_4$ , while the negative electrode consists of LIBs-type materials such as hard carbon, LTO and graphite. The entire charging and discharging process involves a combination of  $\text{Li}^+$  consumption and transmission mechanisms.

Currently reported LICs mainly focus on the first configuration of LIBs-type negative electrode//SCs-type positive electrode. The latter two configurations are relatively less common. Therefore, the LICs mentioned below, unless otherwise specified, belong to the configuration of LIBs-type negative electrode//SCs-type positive electrode.

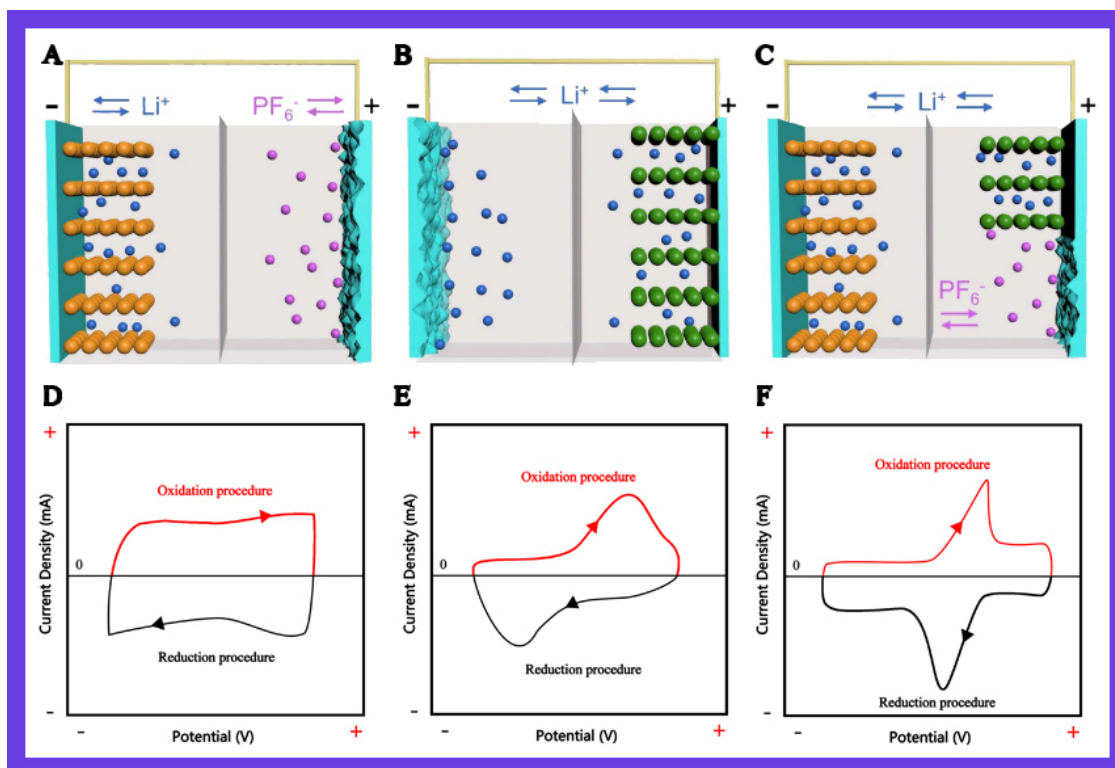


**Figure 2.** LICs with different configurations: (A) LIBs-type negative electrode//SCs-type positive electrode, (B) SCs-type negative electrode//LIBs-type positive electrode, and (C) LIBs-type negative electrode//LIBs-type composite SCs-type positive electrode. Reproduced with permission<sup>[95]</sup>. Copyright 2020, Wiley-VCH.; theoretical CV curves of (D) LIBs-type negative electrode//SCs-type positive electrode, (E) SCs-type negative electrode//LIBs-type positive electrode, and (F) LIBs-type negative electrode//LIBs-type composite SCs-type positive electrode.

## TWO-DIMENSIONAL ANODE MATERIALS FOR LITHIUM-ION CAPACITOR

The 2D materials, such as graphene, TMOs, TMDs, and MXenes, exhibit several distinct advantages over traditional anode materials used in LICs. One of the primary benefits is their exceptionally high surface area, attributed to their planar structure, which provides numerous active sites for  $\text{Li}^+$  storage, thereby enhancing the overall capacity and performance of the capacitor. Additionally, 2D materials are known for their mechanical flexibility, which allows them to withstand significant deformation without breaking. This flexibility is crucial for improving cycling stability and extending the lifespan of LICs, as it helps the anode material accommodate volume changes during charge and discharge cycles. Another notable advantage is the high electrical conductivity of many 2D materials, which ensures efficient electron transport, reducing internal resistance and enhancing the rate capability and PD of the capacitor. Moreover, the properties of 2D materials can be finely tuned through various methods such as doping, functionalization, and adjusting the layer number and stacking. This tunability enables the optimization of material properties to achieve specific performance goals, such as increased ionic conductivity or higher specific capacity. These 2D materials also possess unique structural features, including single or few-layer thickness, which can be leveraged to shorten the diffusion paths for ions and electrons, resulting in faster charge and discharge rates and better performance at high currents. Their lightweight nature further contributes to the development of lightweight energy storage devices (ESDs), which is essential for applications in portable electronics and electric vehicles<sup>[79,96,97]</sup>.

## Graphene

### *Pure graphene*

Graphene, a remarkable 2D material composed entirely of a monolayer of carbon atoms, is the basic component of graphite. Each carbon atom within this lattice is covalently bonded to three others, forming a robust and conductive network. In the context of LIBs<sup>[98,99]</sup>, graphite, derived from stacked graphene layers, is extensively utilized as the anode because of its superior cycling stability. Theoretical calculations reveal that in graphite, each hexagon of six carbon atoms can host one  $\text{Li}^+$ , forming a stable  $\text{LiC}_6$  structure. This interaction provides graphite with a theoretical capacity of  $372 \text{ mAh}\cdot\text{g}^{-1}$ <sup>[100]</sup>. The electrochemical performance of graphite as a negative electrode is profoundly influenced by the arrangement of its graphene layers. Specifically, the spacing between these layers is critical; optimal layer spacing, determined to be between 0.77 and 0.83 nm, facilitates efficient  $\text{Li}^+$  intercalation<sup>[101]</sup>. When this inter-layer distance is maintained within the optimal range, it allows for more rapid insertion of  $\text{Li}^+$ , potentially enhancing the capacity significantly to as much as  $744 \text{ mAh}\cdot\text{g}^{-1}$  - more than twice as many as that of graphite<sup>[102]</sup>. Therefore, enhancing the carbon negative electrode should be achieved by controlling the preparation method of graphene layers.

Graphite can undergo a transformative process through oxidation treatment, resulting in oxidized graphene sheets capable of dispersing in aqueous solutions<sup>[103,104]</sup>. These oxidized sheets can then be reduced using hydrazine chemistry to produce graphene sheets with thicknesses typically ranging from 3 to 7 nm. When utilized as a negative electrode material in LIBs, these reduced graphene sheets demonstrate a significantly enhanced capacity ( $540 \text{ mAh}\cdot\text{g}^{-1}$ ), surpassing the capacity of traditional graphite. Further improvements in lithium storage capacity are achievable by integrating these reduced graphene sheets with other carbon-based materials. Specifically, when combined with carbon nanotubes (CNT) or fullerene (C60), the lithium storage capacities can achieve 730 and  $784 \text{ mAh}\cdot\text{g}^{-1}$ , respectively. This increase is supported by a notable expansion in the interlayer spacing between graphene sheets within these composites - measured at 0.40 nm with CNT and 0.42 nm with C60, compared to 0.365 nm in reduced oxidized graphene alone [Figure 3A-C]<sup>[85]</sup>.

Graphene materials have shown the potential to exceed their theoretical capacity limits, a phenomenon often attributed to the extra active points provided by structural defects and lattice edges in graphene<sup>[109]</sup>. However, the employment of graphene as an anode in LICs faces significant challenges owing to the formation of solid electrolyte interphase (SEI), because a significant amount of  $\text{Li}^+$  are consumed in the formation of the SEI layer, resulting in a lower-than-expected overall capacity and performance of the LICs<sup>[110-112]</sup>. To address these issues, the implementation of a pre-lithiation process has become almost essential. By pre-lithiation, the irreversible  $\text{Li}^+$  consumption during SEI formation is reduced, leading to improved initial capacity, and along with the intercalation of  $\text{Li}^+$ , the overall potential of the graphene anode is reduced, enabling it to operate in a broader voltage range<sup>[113-119]</sup>.

In a comparative operation studied by Ren *et al.*, the electrochemical properties of graphene and graphite were evaluated as anodes for LICs after undergoing an electrochemical pre-lithiation process<sup>[105]</sup>. The study, conducted within 2.0-4.0 V and at  $0.4 \text{ A}\cdot\text{g}^{-1}$ , demonstrated that pre-lithiated graphene exhibited a significantly higher reversible capacity of  $760 \text{ mAh}\cdot\text{g}^{-1}$  compared to graphite ( $370 \text{ mAh}\cdot\text{g}^{-1}$ ). Moreover, when pre-lithiated graphene was used in conjunction with AC in a LIC device, the performance metrics were impressive. The PD of the device reached  $222.2 \text{ W}\cdot\text{kg}^{-1}$  while maintaining an ED of  $67 \text{ Wh}\cdot\text{kg}^{-1}$ . Remarkably, the ED could be sustained at  $98.1 \text{ Wh}\cdot\text{kg}^{-1}$  even when the PD was reduced to  $18 \text{ W}\cdot\text{kg}^{-1}$  [Figure 3D]. This showcases the effectiveness of the pre-lithiation methods in enhancing the electrochemical performance of graphene and highlights its potential in improving the overall efficiency and capacity of LICs.

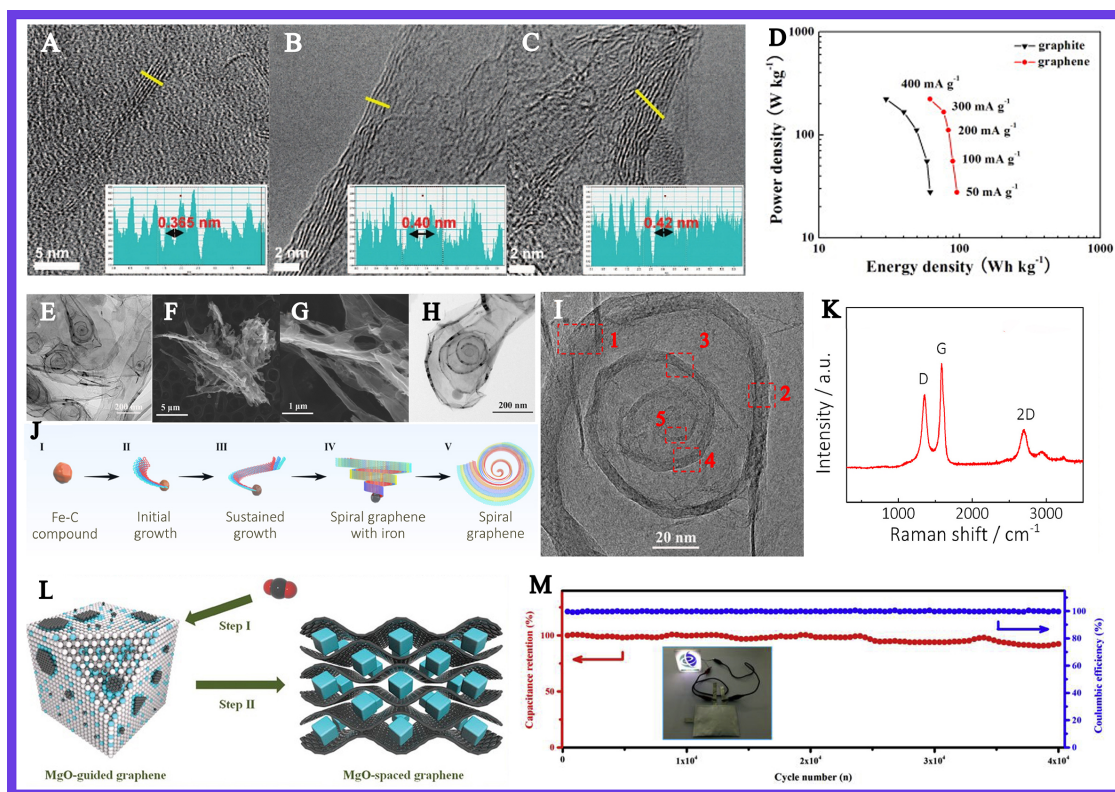


**Figure 3.** (A-C) TEM images of graphene, graphene-CNT, and graphene-C60. Reproduced with permission<sup>[85]</sup>. Copyright 2008, American Chemical Society; (D) Ragone plot of pre-lithiated graphene//AC. Reproduced with permission<sup>[105]</sup>. Copyright 2014, Elsevier B.V.; (E-G) SEM, (H) TEM, (I) HR-TEM images of SG-1000; (J) Formation of spiral graphene; (K) Raman spectra of SG-1000. Reproduced with permission<sup>[106]</sup>. Copyright 2021, Elsevier B.V.; (L) The roles of MgO in forming few-layered graphene. Reproduced with permission<sup>[107]</sup>. Copyright 2016, WILEY-VCH; (M) Cyclic stability of NHCN//SHSG. Reproduced with permission<sup>[108]</sup>. Copyright 2018, Elsevier B.V.

Currently, commercialized carbon negative electrode materials for LICs suffer from a significant drawback: the lithium intercalation potential of graphene is between 0.1–0.5 V, which is higher than the graphite negative electrode and reduces the ED of the LICs. Therefore, it is necessary to explore new types of graphene materials and improve their graphitization degree to lower lithium insertion potential and achieve high-rate performance<sup>[120,121]</sup>.

Spiral Graphene (SG) is synthesized by Wang *et al.*, through an innovative process that transforms carboxymethyl chitosan, a biopolymer derivative, using a chloride-molten-salts treatment<sup>[106]</sup>. Initially, the SG displays a fibrous morphology; however, as the calcination temperature increases, a fascinating transformation occurs. Embedded within a matrix at lower temperatures, these fibers begin to peel off and gradually become exposed on the surface as the temperature reaches 1,000 °C [Figure 3E]. At this high calcination temperature, the fibrous structures undergo a substantial morphological change, evolving into nano-coils [Figure 3F–H]. Within these nano-coils, macroscopic pores are present, which are pivotal for enhancing the electrochemical properties of the material. These pores allow the electrolyte to fully penetrate the surface of the active material, effectively reducing the diffusion pathway for ions and enhancing the material's functionality in LICs. Moreover, a notable structural feature of the spiral graphene is the gradual decrease in the number of graphene layers from the edge toward the center of the spiral [Figure 3I]. This gradient in layer thickness could be attributed to the dynamics of the catalyst during the catalytic graphitization process, which possibly undergoes a spiral motion [Figure 3J]. This unique feature further



highlights the complex interplay between the synthesis conditions and the resulting morphology and properties of the resulting carbon materials. SG exhibits a unique helical structure complemented by high graphitization and a porous framework, key structural characteristics that significantly enhance their electrochemical performance. One of the standout features of SG is its high reversible capacity, achieving  $403 \text{ mAh}\cdot\text{g}^{-1}$  at  $0.05 \text{ A}\cdot\text{g}^{-1}$  within  $0.01\text{-}2.0 \text{ V vs. Li}^+/\text{Li}$ . This high capacity underscores its considerable potential in energy storage applications.

Raman spectroscopy [Figure 3K] analysis of SG-1000 reveals  $I_G/I_D = 1.03$ , indicative of a well-aligned graphene structure. Such alignment contributes to an increased plateau capacity, maintains stable negative potential, and maximizes the voltage range for the positive electrode in LICs. In a practical LIC setup pairing SG-1000 with hierarchically porous carbon-10 (HPC-10), the materials achieve an impressive ED of  $57 \text{ Wh}\cdot\text{kg}^{-1}$  and a PD of  $6,323 \text{ W}\cdot\text{kg}^{-1}$  within  $2.0\text{-}4.2 \text{ V}$ . These metrics confirm the efficacy of SG in high-performance LICs. Additionally, the cyclic stability of the SG-1000//HPC-10 LICs is remarkable, retaining 90.3% of their capacity after 10,000 cycles at  $5 \text{ A}\cdot\text{g}^{-1}$ , across  $2.0\text{-}4.0 \text{ V}$ . This durability is essential for applications demanding longevity and reliability, further highlighting the potential of SG in future energy storage systems (ESSs).

The commercial viability of graphene primarily depends on its effective synthesis in large-scale industrial settings, in addition to enhancing the quality of graphene itself. To date, the two-step method has been the primary approach for graphene production. However, these methods employ environmentally unfriendly reagents, simultaneously introducing numerous structural defects that lower conductivity. Furthermore, based on the influence of interlayer  $\pi\text{-}\pi$  interactions, graphene tends to aggregate during electrode preparation, diminishing its SSA and ion diffusion rate, leading to suboptimal capacitance ( $< 180 \text{ F}\cdot\text{g}^{-1}$ ) and low PD<sup>[110]</sup>.

Herein, Li *et al.* explored a novel synthesis way for a unique type of graphene, known as self-propagating high-temperature synthesis-prepared graphene-8 (SHSG-8), utilizing a superfast, eco-friendly, and scalable self-propagating approach<sup>[107]</sup>. This method incorporates MgO, which plays a crucial role in offering active points for graphene growth while simultaneously preventing the aggregation of graphene layers, thereby facilitating the output of high-quality graphene [Figure 3L]. The resultant SHSG-8 graphene is characterized by its unique interconnected framework, remarkably low oxygen content (less than 1 at.%), and high conductivity ( $13,000 \text{ S}\cdot\text{m}^{-1}$ ). In terms of electrochemical performance, SHSG-8 showcases  $845 \text{ mAh}\cdot\text{g}^{-1}$  at  $0.15 \text{ A}\cdot\text{g}^{-1}$ , significantly surpassing the performance of commercial graphite by 2.3 times within  $0.01$  to  $3.0 \text{ V vs. Li}^+/\text{Li}$ <sup>[108]</sup>. Additionally, the charge-discharge curves of SHSG-8 show no plateaus and are characterized by a capacity that is mainly derived from voltages below  $1.0 \text{ V}$  across a range of current densities. When used in lithium-ion capacitors (LICs), SHSG-8, coupled with nitrogen-doped hierarchical carbon nanolayer (NHCN) cathodes, achieves impressive ED of  $146$  and  $103 \text{ Wh}\cdot\text{kg}^{-1}$  at PD of  $650 \text{ W}\cdot\text{kg}^{-1}$  and  $52 \text{ kW}\cdot\text{kg}^{-1}$ , respectively, within  $2$  to  $4.5 \text{ V}$ . After 40,000 cycles, the LICs also retain remarkable 91% capacity retention at  $4 \text{ A}\cdot\text{g}^{-1}$  [Figure 3M]. In conclusion, the innovative synthesis of SHSG-8 not only results in graphene with superior electrochemical properties but also significantly enhances the performance of LICs.

However, pure graphene has a tendency to restack owing to van der Waals forces or other interactions, substantially reducing its effective surface area available for reactions. This limitation hinders the provision of adequate active sites necessary for electrochemical reactions, thereby diminishing its energy storage capacity. Consequently, a key method being explored is the doping of graphene with various elements. This technique involves introducing impurities into the graphene lattice, which alters its electrical properties, thereby potentially enhancing its performance as an anode material. Another innovative strategy is the



development of composite materials. This approach seeks to capitalize on the unique benefits of graphene, such as its high conductivity and large SSA, along with the advantageous performance characteristics of other materials, to produce anodes that are more efficient and capable.

### *Doped graphene*

Graphene sheets, due to their unique 2D structure, have the potential to significantly enhance lithium storage capabilities. Unlike commercial bulk graphite, which accommodates  $\text{Li}^+$  only between its layered structure, graphene can theoretically bind  $\text{Li}^+$  on both sides of its plane. This dual-sided binding capability not only has the potential to double the adsorption capacity of graphene but also shortens the  $\text{Li}^+$  transmission path, thereby accelerating  $\text{Li}^+$  insertion/extraction. This makes graphene potentially more suitable for reversible lithium storage compared to commercial bulk graphite.

However, the practical application of monolayer graphene in lithium storage faces significant challenges. Although theoretically advantageous, reports have shown that the actual lithium coverage on the surface of monolayer graphene is lower than expected. This reduced adsorption capacity is primarily attributed to two main factors. Firstly, the binding energy between  $\text{Li}^+$  and the carbon atoms of graphene is lower than that in other carbon forms. This weaker interaction results in less stable lithium adsorption on the graphene surface. Secondly, strong Coulomb repulsion between lithium atoms situated on opposite sides of the graphene sheet complicates this scenario further. This repulsion can hinder the effective utilization of both sides of the graphene for lithium storage, preventing graphene from reaching its full potential in  $\text{Li}^+$  applications<sup>[122,123]</sup>. Additionally, the high diffusion barrier accumulated by  $\text{Li}^+$  in multilayer graphene also impedes lithium diffusion on the graphene plane. Fortunately, heteroatom dopants can significantly improve the aforementioned issues, and doping with heteroatoms can effectively prevent graphene from re-aggregation and clustering, as enhanced polarity can greatly reduce the surface tension and  $\pi$ - $\pi$  interactions of graphene<sup>[124,125]</sup>.

Nitrogen doping, as a significant means of modifying carbon materials, presents several advantages. Primarily, due to its inherent electrical conductivity and atomic size similar to that of carbon, nitrogen is readily incorporated into carbon materials, maintaining excellent stability<sup>[126-130]</sup>. Furthermore, nitrogen doping enhances the interaction between carbon materials and  $\text{Li}^+$ , thereby increasing the  $\text{Li}^+$  coverage of electrode materials and promoting reversible  $\text{Li}^+$  cycling<sup>[131-134]</sup>. Additionally, this technique improves the electronic conductivity of carbon materials, and lowers the diffusion barrier for ions, thereby facilitating the penetration of  $\text{Li}^+$  within electrode materials.

What is more, nitrogen doping actually provides more active points for  $\text{Li}^+$  storage. These additional sites are crucial for increasing the charge storage capacity of the materials, making nitrogen doping a pivotal technique in the development of advanced electrode materials<sup>[124,135,136]</sup>. Therefore, this method holds significant importance in increasing the charge storage capacity of carbon materials. The study by Tian *et al.* further exemplifies the practical applications of this technique<sup>[80]</sup>. They synthesized nitrogen-doped graphene sheets (NGSs) using glucose as a precursor through a top-down approach, effectively incorporating different types of nitrogen configurations - namely pyridinic (N-6), graphitic (N-Q), and pyrrolic (N-5) nitrogen - into the graphene lattice [Figure 4A]. This method resulted in graphene sheets with a high SSA of  $504 \text{ m}^2\cdot\text{g}^{-1}$ . When tested, these sheets exhibited a remarkable electrochemical performance, achieving  $832.4 \text{ mAh}\cdot\text{g}^{-1}$  at  $0.1 \text{ A}\cdot\text{g}^{-1}$  within 0.05 to 3 V vs.  $\text{Li}^+/\text{Li}$ . Similarly, Ma *et al.* employed  $\text{NH}_3$  and porous MgO as the nitrogen source and substrate, respectively, to prepare nitrogen-doped graphene [nitrogen-doped mesoporous graphene (NMG)] [Figure 4B]<sup>[81]</sup>. During the growth of graphene, nitrogen was concurrently introduced into the carbon lattice in situ, ensuring the uniformity of nitrogen

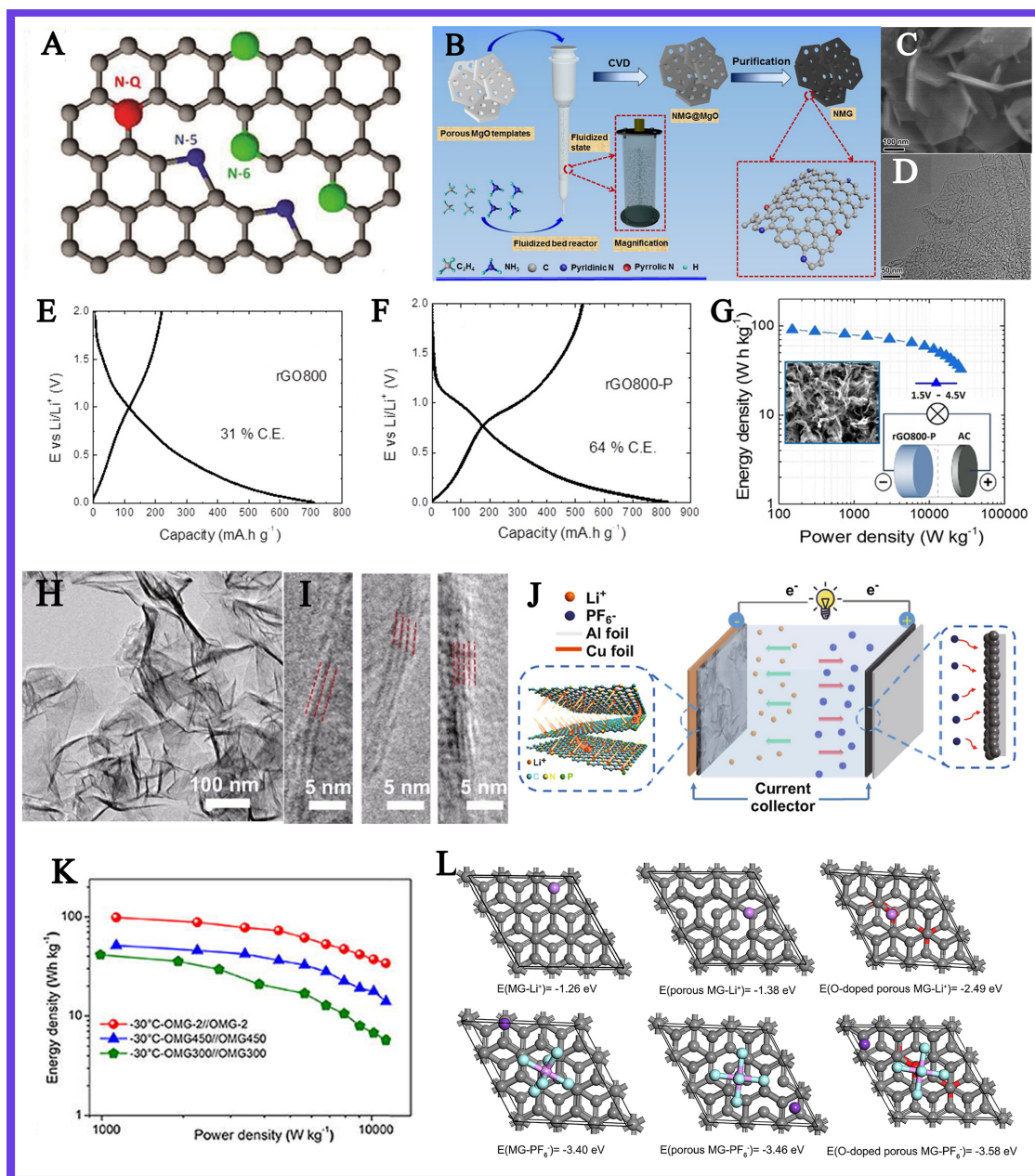


**Figure 4.** (A) Possible positions of pyridine (N-6), graphite (N-Q), and pyridine (N-5) nitrogen in the carbon skeleton. Reproduced with permission<sup>[80]</sup>. Copyright 2014, The Royal Society of Chemistry; (B) Preparation process of NMG; (C) SEM and (D) TEM image of NMG. Reproduced with permission<sup>[81]</sup>. Copyright 2018, American Chemical Society; (E) GCD curves for the first cycle and at different current rates for rGO800 (E) and rGO800-P (F); (G) Ragone plot of rGO800-P//AC LICs. Reproduced with permission<sup>[82]</sup>. Copyright 2020, Wiley-VCH; (H) SEM and (I) TEM image of NPG; (J) Construction of NPG//AC LICs. Reproduced with permission<sup>[83]</sup>. Copyright 2019, Springer Nature; (K) Ragone plot of OMG-2//OMG-2 LICs; (L) The DFT calculation models after Li<sup>+</sup> and PF<sub>6</sub><sup>-</sup> absorption. Reproduced with permission<sup>[137]</sup>. Copyright 2021, Elsevier B.V.

doping. The unique microstructure of NMG can effectively reduce aggregation or rearrangement tendencies [Figure 4C and D]. The capacity of NMG performed 220 mAh·g<sup>-1</sup> at 0.5 A·g<sup>-1</sup> within 0.01–1.5 V (vs. Li<sup>+</sup>/Li). The NMG//NMG LICs have resulted in a high ED of 128 and 92 Wh·kg<sup>-1</sup> obtained at 500 W·kg<sup>-1</sup> and 10 kW·kg<sup>-1</sup>, spanning 0.01–4.0 V. Additionally, the LICs exhibited remarkable cycling durability (98.3% after 4,000 cycles) when tested at 3 A·g<sup>-1</sup> between 0.01–4.0 V.

Apart from nitrogen atom doping, other heteroatoms can also change electronic structure and induce interlayer expansion. When atoms with different electronegativities and radii are doped into a material, they can alter its fundamental attributes. For instance, the electronegativity of the doped atoms affects the electronic structure of the host material, influencing its ability to attract and hold onto electrons. This, in turn, can modify the material's electrical conductivity. Similarly, the atomic radius of the doped atoms influences the spatial configuration and density of the material. Larger atoms might expand the lattice structure of the material, potentially creating more active sites, which are beneficial for reactions in catalytic processes or energy storage applications. Conversely, smaller atoms may fit more discreetly into the lattice, affecting the material's density and mechanical properties. As a result of these modifications, the material might exhibit varied quantities of active points, influencing its reactivity and effectiveness in specific applications<sup>[138,139]</sup>. For example, the doping or functionalization of phosphorus induces topological defects with higher electron-donating capability compared to carbon, thereby accelerating the kinetics of lithium storage and transport<sup>[140,141]</sup>. Moreno-Fernández *et al.* prepared phosphorus-functionalized graphene (rGO800-P) by thermal reduction by using graphene oxide (GO) and concentrated phosphoric acid as raw materials<sup>[82]</sup>. As depicted in Figure 4E and F, the coulombic efficiency (C.E.) increases from 31% (rGO800) to 64% (rGO800-P), which demonstrated that phosphorus functionalization effectively reduces the degree of irreversible reactions. This outcome can be owing to the lower SSA of rGO800-P and phosphorus occurring at the edge plane sites, which may reduce the amount of irreversibly captured lithium and enhance electron transport within the sample. And during 0.01-2.0 V vs. Li<sup>+</sup>/Li, rGO800-P can showcase 461 mAh·g<sup>-1</sup> at 5 A·g<sup>-1</sup>, much than that of rGO800 (252 mAh·g<sup>-1</sup>). The fabricated rGO800-P//AC LICs [Figure 4G] achieved a maximum ED of 91 Wh·kg<sup>-1</sup> at the PD of 145 W·kg<sup>-1</sup> and retaining 33 Wh·kg<sup>-1</sup> at 26 kW·kg<sup>-1</sup>, with a capacitance retention of 76% after 10,000 cycles (at 5 A·g<sup>-1</sup> from 1.5 to 4.5 V). In addition, Luan *et al.* utilized (NH<sub>4</sub>)<sub>3</sub>PO<sub>4</sub> as the nitrogen-phosphorus source to synthesize nitrogen-phosphorus dual-doped graphene (NPG) via a one-step arc discharge method under a mixed atmosphere of He and H<sub>2</sub><sup>[83]</sup>. The NPG nanosheets primarily consist of 2-6 layers of graphene, with phosphorus and nitrogen concentrations of 1.3 and 3.2 at.%, respectively, and exhibit a naturally wrinkled and curled layered petal-like morphology [Figure 4H]. As depicted in Figure 4I, a majority of graphene consists of six sheets or fewer. During 0.01-3.0 V vs. Li<sup>+</sup>/Li, NPG can deliver 758 mAh·g<sup>-1</sup> at 2 A·g<sup>-1</sup>. The fabricated NPG//AC LICs [Figure 4J] achieved a maximum ED of 195 Wh·kg<sup>-1</sup> at the PD of 746.2 W·kg<sup>-1</sup> and retaining 77 Wh·kg<sup>-1</sup> at 14,983.7 W·kg<sup>-1</sup>, with an exceptional capacitance retention of 94.2% after 5,000 cycles (at 1 A·g<sup>-1</sup> from 1.0 to 4.0 V). The introduction of both N and P into the graphene structure significantly increases the number of active points available for Li<sup>+</sup> storage. The additional sites allow for more Li<sup>+</sup> to be stored during charging processes, which, in turn, contributes to higher energy densities and potentially faster charging times. Thus, the combination of nitrogen and phosphorus doping in graphene not only enhances its intrinsic electrical properties but also substantially improves its functionality as a lithium storage material, demonstrating why NPG stands out for its outstanding electrochemical performance.

Oxygen doping emerges as a pivotal and extensively researched method in the heteroatom doping of carbon-based materials, particularly important for those with high surface areas where the inclusion of oxygen heteroatoms is nearly inevitable. This doping strategy involves the deliberate introduction of oxygen-containing functional groups, such as hydroxyl, carbonyl, and epoxide groups, onto the surface of carbon materials. These functional groups have a profound influence on the electrochemical properties of the materials, exerting impact on aspects such as electrode reactivity and ion-exchange capacities. Oxygen functional groups are instrumental in improving the electrochemical characteristics of materials, primarily through the induction of reversible faradaic reactions which contribute to increased pseudo-capacitance. Additionally, these groups enhance the surface wettability of the material, facilitating better interactions between the electrode and the electrolytes, which is crucial for optimizing the efficiency of ESDs. However, the introduction of oxygen functional groups must be carefully controlled. While they offer significant

benefits in terms of increasing capacitance and improving wettability, there is a critical balance that needs to be maintained. An overabundance of oxygen can lead to a decrease in the overall conductivity of the material, detracting from its electrochemical performance. Therefore, managing the level of oxygen functional groups is essential to maximize their positive effects without compromising the material's conductivity.

In conclusion, while oxygen doping is recognized for its ability to strengthen the functionality and performance of carbon-based electrodes through improvements in pseudo-capacitance and wettability, careful control over the extent of doping is essential. This ensures that the advantages of oxygen functional groups are maximized without compromising the material's conductivity, thereby optimizing the electrochemical performance of the electrode materials<sup>[142,143]</sup>.

By carefully controlling the reaction conditions, Xiao *et al.* synthesized O-doping multilayered porous graphene (OMG) nanosheets characterized by a high SSA ( $683.8 \text{ m}^2\cdot\text{g}^{-1}$ )<sup>[137]</sup>, abundant nanoscale pores, expanded graphene interlayer spacing, and outstanding dispersion. Between 0.01-1.6 V, OMG offered  $247 \text{ mAh}\cdot\text{g}^{-1}$  at  $1 \text{ A}\cdot\text{g}^{-1}$  and  $138 \text{ mAh}\cdot\text{g}^{-1}$  even at  $10 \text{ A}\cdot\text{g}^{-1}$ , which showed a better outstanding rate performance. The resulting OMG-based LICs showed  $131.6 \text{ Wh}\cdot\text{kg}^{-1}$  at  $2,272 \text{ W}\cdot\text{kg}^{-1}$  and  $87.3 \text{ Wh}\cdot\text{kg}^{-1}$  at  $21.66 \text{ kW}\cdot\text{kg}^{-1}$  [Figure 4K], as well as superior capacity retention (96.8% after 5,000 cycles within 0.01-4 V). Additionally, the study meticulously investigates the effects of oxygen doping on the electronic performance of multilayered porous graphene, particularly focusing on the adsorption of  $\text{Li}^+$  and  $\text{PF}_6^-$  ions. Utilizing Density Functional Theory (DFT) computational models [Figure 4L], the research analyzed three distinct types of graphene materials: pure multilayer graphene (MG), porous MG (PMG), and oxygen-doped porous MG (OPMG). The findings reveal a clear trend in the adsorption energies: for  $\text{Li}^+$ , the adsorption energies were  $-1.26 \text{ eV}$  for MG,  $-1.38 \text{ eV}$  for PMG, and a much more negative  $-2.49 \text{ eV}$  for OPMG. This significant increase in negativity with oxygen doping underscores its effectiveness in enhancing  $\text{Li}^+$  adsorption.

Similarly, the adsorption energies for  $\text{PF}_6^-$  followed a comparable pattern, being  $-3.40 \text{ eV}$  for MG,  $-3.46 \text{ eV}$  for PMG, and the most negative at  $-3.58 \text{ eV}$  for OPMG. These results further corroborate that oxygen doping not only benefits the adsorption of  $\text{Li}^+$  but also positively influences the adsorption of  $\text{PF}_6^-$ , suggesting an overall enhancement in the electronic performance of the graphene materials due to the presence of oxygen.

#### Graphene composite

The composite engineering, achieved by combining materials with complementary properties, enables synergistic effects leading to enhanced electrochemical performance. This strategy garners considerable attention in the current realm of material performance optimization. Each component within composite materials can mutually compensate for deficiencies and leverage its respective strengths, thereby improving overall performance. For instance, the integration of graphene with other functional materials, such as conductive polymers or metal oxides, can effectively extend the lifespan and stability of electrodes. Moreover, by controlling the structure and composition of composite materials, one can modulate their electron and ion transport rates, further optimizing electrochemical performance. Overall, composite engineering provides crucial insights and methodologies for the design of more efficient and superior electrochemical materials<sup>[144]</sup>.

Transition metal selenides have proved to be very potential LIBs-type materials because of their fast reaction rates and abundant theoretical capacity<sup>[145]</sup>. Among them, cobalt selenide ( $\text{CoSe}_2$ ) has garnered significant attention as a key member owing to its outstanding conductivity and high theoretical capacity ( $494.4 \text{ mAh}\cdot\text{g}^{-1}$ ). However,  $\text{CoSe}_2$  experiences severe volume changes during conversion reactions, leading to



structural fragmentation issues and rapid capacity decay, thus resulting in cycling instability. To address this challenge, a recent strategy involving heterogeneous structure has been put forward to hold the structural stability of CoSe<sub>2</sub> and enhance its cycling lifespan. Such heterogeneous structures are typically composed of different components stacked together, possessing unique interfaces that facilitate synergistic effects through close contact and interface interactions. Moreover, structural changes at heterogeneous interfaces can generate additional electrocatalytic active points onto the electrode<sup>[92]</sup>. In a significant study by Wei *et al.*, researchers successfully developed and characterized a novel composite material, CoSe<sub>2</sub>/N-doped reduced GO (CoSe<sub>2</sub>/N-rGO), using flexible graphene as a substrate while GO and basic cobalt carbonate as precursors through interface engineering methods<sup>[89]</sup>. This approach led to the successful preparation of the composite where CoSe<sub>2</sub> nanoparticles are tightly bonded to the N-doped graphene, preserving the original 2D structure similar to an earlier material (CoCH/rGO) [Figure 5A and B]. During the selenization process, initially formed Co(OH)<sub>0.5</sub>CO<sub>3</sub> nanosheets were transformed into CoSe<sub>2</sub> nanoparticles through a high-temperature decomposition reaction. Microscopic observations, particularly transmission electron microscopy (TEM) images [Figure 5C], showcased a strong interfacial binding between CoSe<sub>2</sub> nanoparticles and the graphene surface, with noticeable grooves and holes on the surface, indicating the structural transformation.

Electrochemically, the CoSe<sub>2</sub>/N-rGO composite demonstrated outstanding performance. It achieved 805.5 mAh·g<sup>-1</sup> at 0.1 A·g<sup>-1</sup> within 0.01 to 3 V vs. Li<sup>+</sup>/Li. When acted as an anode material in LICs paired with AC cathodes, the composite showed an impressive ED of 104.2 Wh·kg<sup>-1</sup> and a PD of 5,452.7 W·kg<sup>-1</sup>. Moreover, it displayed excellent cycling stability, retaining 81.2% of its capacity after 8,000 cycles at 1 A·g<sup>-1</sup> within 1.0 to 4.2 V [Figure 5D and E].

Recently, the Ti<sub>x</sub>Nb<sub>y</sub>O<sub>z</sub>-type mixed metal oxides have attracted widespread attention. These materials exhibit characteristics similar to LTO, such as a high operating potential (~1.7 V), low volume change, and excellent rate capability. Compared to LTO, Ti<sub>x</sub>Nb<sub>y</sub>O<sub>z</sub> materials possess a higher Li<sup>+</sup> diffusion coefficient owing to their open Wadsley-Roth shear structure, which provides superior rate performance<sup>[146,147]</sup>. Additionally, during Li<sup>+</sup> insertion/extraction processes, the high lithium intercalation potential (~1.7 V) contributes to additional safety by suppressing the formation of SEI/lithium dendrites. Particularly noteworthy is that TiNb<sub>6</sub>O<sub>17</sub> (TNO, 397 mAh·g<sup>-1</sup>) shares the same crystal structure as Ti<sub>2</sub>Nb<sub>10</sub>O<sub>29</sub> (396 mAh·g<sup>-1</sup>), but the former has larger cation vacancies and lattice parameters, resulting in a higher Li<sup>+</sup> diffusion coefficient. However, the lower conductivity of the TNO anode leads to capacity decay<sup>[148-151]</sup>. Therefore, Chaturvedi *et al.* introduce a composite material known as R-TNO, consisting of TNO particles uniformly distributed on reduced GO (rGO) sheets<sup>[48]</sup>. This was synthesized using a time-efficient, cost-effective, and scalable solid-state reaction, aiming to strengthen the electrochemical properties of the material in LICs. The structural and surface analysis of R-TNO [Figure 5F-H] shows an apparent increase in SSA to 18.8 m<sup>2</sup>·g<sup>-1</sup> compared to the 10.6 m<sup>2</sup>·g<sup>-1</sup> of pristine TNO, attributed to the presence of nano-pores on the rGO sheets. Additionally, the material features a porous structure with a pore volume of 0.209 cm<sup>3</sup>·g<sup>-1</sup> and mesoporous characteristics with 44.3 nm pores, which significantly improve ion transport. The R-TNO electrode also exhibits enhanced hydrophilicity due to various functional groups and edge components on the rGO sheets, which promote better electrode-electrolyte interactions [Figure 5I and J]. This improved hydrophilicity contributes to enhanced redox activity by making more active sites available and allows for strong bonding with electrolyte ions through the functional groups on the rGO, thus boosting the electrochemical properties. In practical terms, R-TNO demonstrates 365 mAh·g<sup>-1</sup> at 3.97 A·g<sup>-1</sup> compared to the TNO (301 mAh·g<sup>-1</sup>), marking it as a more efficient anode material for high-rate applications. When utilized as an anode in LICs with AC as the cathode, the assembled LICs delivered impressive ED of 142.1 Wh·kg<sup>-1</sup> at 375 W·kg<sup>-1</sup> and PD of 18.75 kW·kg<sup>-1</sup> at 81 Wh·kg<sup>-1</sup>. Moreover, the R-TNO//AC LIC showed excellent cycling stability, holding 88% after 10,000 cycles at 4.0 A·g<sup>-1</sup> within 0.01 to 3.0 V.



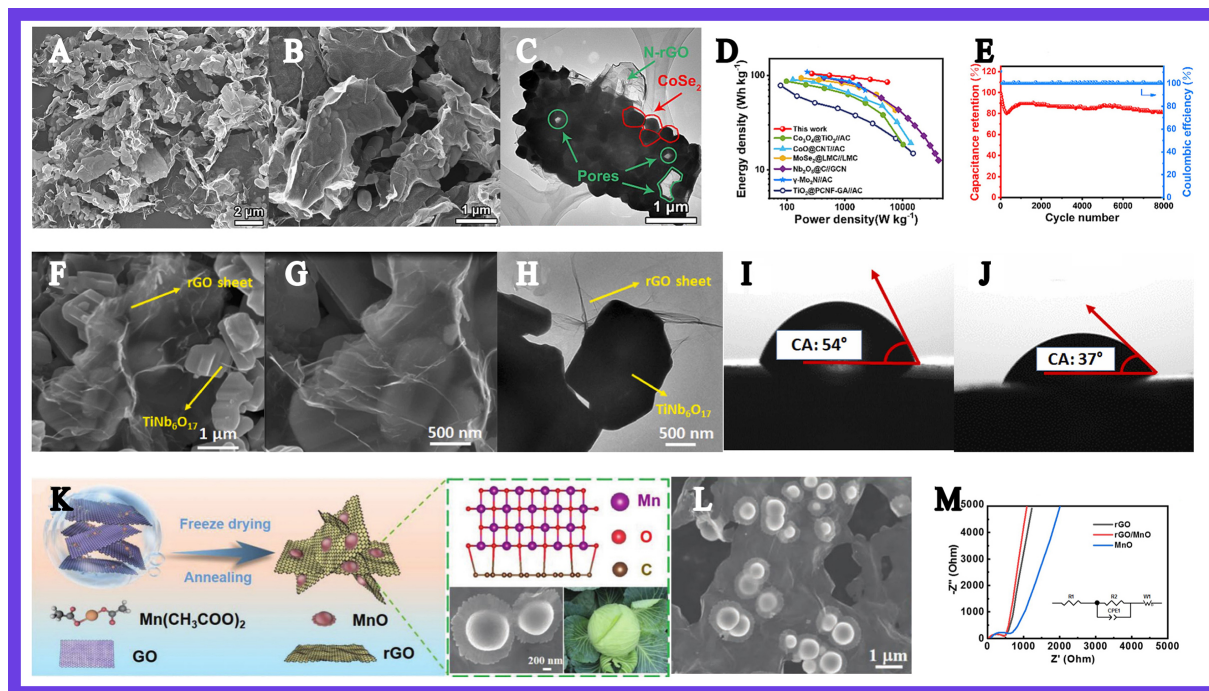


**Figure 5.** (A and B) SEM and (C) TEM of  $\text{CoSe}_2/\text{N-rGO}$ ; (D) Ragone plot of  $\text{CoSe}_2/\text{N-rGO}/\text{AC}$ ; (E) Cyclic stability of  $\text{CoSe}_2/\text{N-rGO}/\text{AC}$ . Reproduced with permission<sup>[89]</sup>. Copyright 2023, Elsevier B.V.; (F and G) SEM and (H) TEM of R-TNO; the contact angle image of the (I) TNO and (J) R-TNO. Reproduced with permission<sup>[48]</sup>. Copyright 2023, Elsevier B.V.; (K) The synthetic route for rGO/MnO; (L) SEM images of rGO/MnO; (M) Nyquist plots of the rGO, MnO, and rGO/MnO. Reproduced with permission<sup>[90]</sup>. Copyright 2022, Wiley-VCH.

Besides, MnO, characterized as a representative conversion-type anode material, demonstrates promising prospects as an advanced anode for LICs due to its high theoretical capacity of  $755 \text{ mAh}\cdot\text{g}^{-1}$ , lower lithium intercalation potential ( $< 0.7 \text{ V}$ ), *etc.*<sup>[152-154]</sup>. However, the intrinsic low electronic conductivity of MnO and the easily re-constructible internal structure led to significant declines of capacity and cycling performance, hindering the further development<sup>[155-157]</sup>. It is reported that GO, when dispersed in an aqueous solution, exhibits electronegative characteristics on its surface<sup>[158]</sup>. Subsequently, materials with heterogeneous structures can be obtained through processes such as hydrothermal treatment or calcination<sup>[159-161]</sup>. Thereby, Liu *et al.* have proposed a universal, controllable, and scalable strategy for synthesizing heterostructure materials composed of MnO and graphene (rGO/MnO), in which graphene serves a dual purpose in enhancing electron transport and facilitating the permeation of electrolytes, all the while serving as a protective layer to maintain structural integrity<sup>[90]</sup>.  $\text{Mn}^{2+}$  is adsorbed on the GO surface by electrostatic action, and forms MnO nanocabbage in situ during subsequent heat treatment, and is anchored to the rGO sheet by Mn-O-C bond [Figure 5K and L]. From Figure 5M, it can be seen that based on the strong Mn-O-C bonds and high conductivity of rGO, it can effectively enhance electron transfer performance and promote ion transport. Therefore, at  $0.1 \text{ A}\cdot\text{g}^{-1}$  (during  $0.01\text{-}3 \text{ V vs. Li}^+/\text{Li}$ ), rGO/MnO showed  $861 \text{ mAh}\cdot\text{g}^{-1}$  and even at  $10 \text{ A}\cdot\text{g}^{-1}$ , it can still provide a high capacity of  $211 \text{ mAh}\cdot\text{g}^{-1}$ . In addition, the rGO/MnO//AC LICs showed excellent ED ( $194.6 \text{ Wh}\cdot\text{kg}^{-1}$  at  $269.3 \text{ W}\cdot\text{kg}^{-1}$ ), ultra PD ( $40.7 \text{ kW}\cdot\text{kg}^{-1}$  at  $57.4 \text{ Wh}\cdot\text{kg}^{-1}$ ) and 77.9% capacity retention after 10,000 cycles, during  $1\text{-}4.4 \text{ V}$ .

In summary, despite graphene demonstrating significant theoretical potential, its large-scale production and practical application still encounter challenges, including issues related to cost, scalability, and environmental friendliness which remain to be addressed. Furthermore, through the rational design of

structures, the introduction of defects, the incorporation of heteroatoms, or composite materials, graphene and its derivatives show significant potential in addressing the kinetic imbalance between the anode and cathode for LICs.

### Transition-metal oxides

The 2D TMOs exhibit chemical and mechanical stability, enhancing ion intercalation while minimizing volume expansion. By rationally designing a 2D structure, the positive and negative volume changes experienced by the material can be stacked in multilayer structures, even further reducing volume change to zero. Zero volume change contributes to the prolongation of energy storage lifespan and stability<sup>[162]</sup>. Additionally, 2D materials possess the considerable interlayer space. This space is not merely a structural feature but a functional advantage that allows for the efficient storage of ions. The combination of significant interlayer space and high packing density leads to a substantial benefit in energy storage applications: a higher volumetric ED<sup>[163,164]</sup>. Moreover, it is possible to modify and enhance the interlayer spacing of 2D TMOs to support the storage of larger ions such as Na<sup>+</sup>, K<sup>+</sup>, Zn<sup>2+</sup>, and Al<sup>3+</sup>, thus extending the storage capacity<sup>[165,166]</sup>. However, the inherent electronic conductivity of oxide materials, which are commonly used in various ESDs, is relatively low. This fundamental property poses a significant challenge in their application because effective energy storage and transfer depend heavily on the material's ability to conduct electrons. To compensate for this deficiency, these oxides are often mixed with additives that possess high electrical conductivity. However, these additives typically do not participate in the electrochemical reactions that store and release energy, serving only to enhance the conductivity of the composite material. This approach, while effective in improving conductivity, has a drawback: it increases the overall weight of the device. The added weight is due to the incorporation of additional materials that do not contribute directly to energy storage, potentially limiting the efficiency and practicality of the device<sup>[165,167,168]</sup>. Given these challenges, one promising approach is using atomically thin, 2D oxides. These materials, often referred to as monolayers, represent the ultimate limit in thinness, typically just one atom thick. This extreme thinness offers several advantages. Firstly, their 2D structure can significantly enhance the surface area available for redox (reduction-oxidation) reactions, which are central to the storage and release of energy in batteries and capacitors. A higher surface area can potentially lead to greater energy storage capacity and faster reaction rates.

Furthermore, these monolayer oxides can be engineered to possess better electronic properties compared to their bulk counterparts. The reduction in dimensionality often affects the electronic structure of materials, sometimes leading to enhanced conductivity. By harnessing these unique properties, monolayer 2D oxides can address the core issue of poor conductivity while maximizing the active surface area, thereby optimizing the material's performance in energy storage applications without the need for additional, inactive additives. This approach not only preserves the lightness and compactness of the ESD but also leverages the advanced capabilities of nanomaterial engineering to overcome traditional material limitations.

Lately, there has been a significant focus on Co-based materials due to their cost-effectiveness and greater abundance compared to noble metal oxides such as RuO<sub>2</sub> and IrO<sub>2</sub>. Co-based materials offer multiple oxidation states that facilitate charge transfer and reversible adsorption, making them ideal electrode materials<sup>[169]</sup>. Specifically, Co<sub>3</sub>O<sub>4</sub>, with its characteristic spinel structure, boasts a high theoretical specific capacitance (3,650 F·g<sup>-1</sup>), outstanding reversibility, affordability, ample availability, and distinct electrochemical redox activity<sup>[170,171]</sup>. Lu *et al.* first synthesized self-assembled cobalt hydroxalate-like compounds (Co-HLC) via the reflux process involving cobaltous nitrate and urea<sup>[172]</sup>. Upon pyrolysis of Co-HLC, its distinctive flower-like structure is effectively preserved in the resulting well-organized 2D Co<sub>3</sub>O<sub>4</sub> nanosheets [Figure 6A-C], ensuring favorable electrolyte contact and a stable porous framework throughout the lithiation/de-lithiation process. At a 0.04 A·g<sup>-1</sup>, during 0.01-3 V (vs. Li<sup>+</sup>/Li), the Co<sub>3</sub>O<sub>4</sub> nanosheets

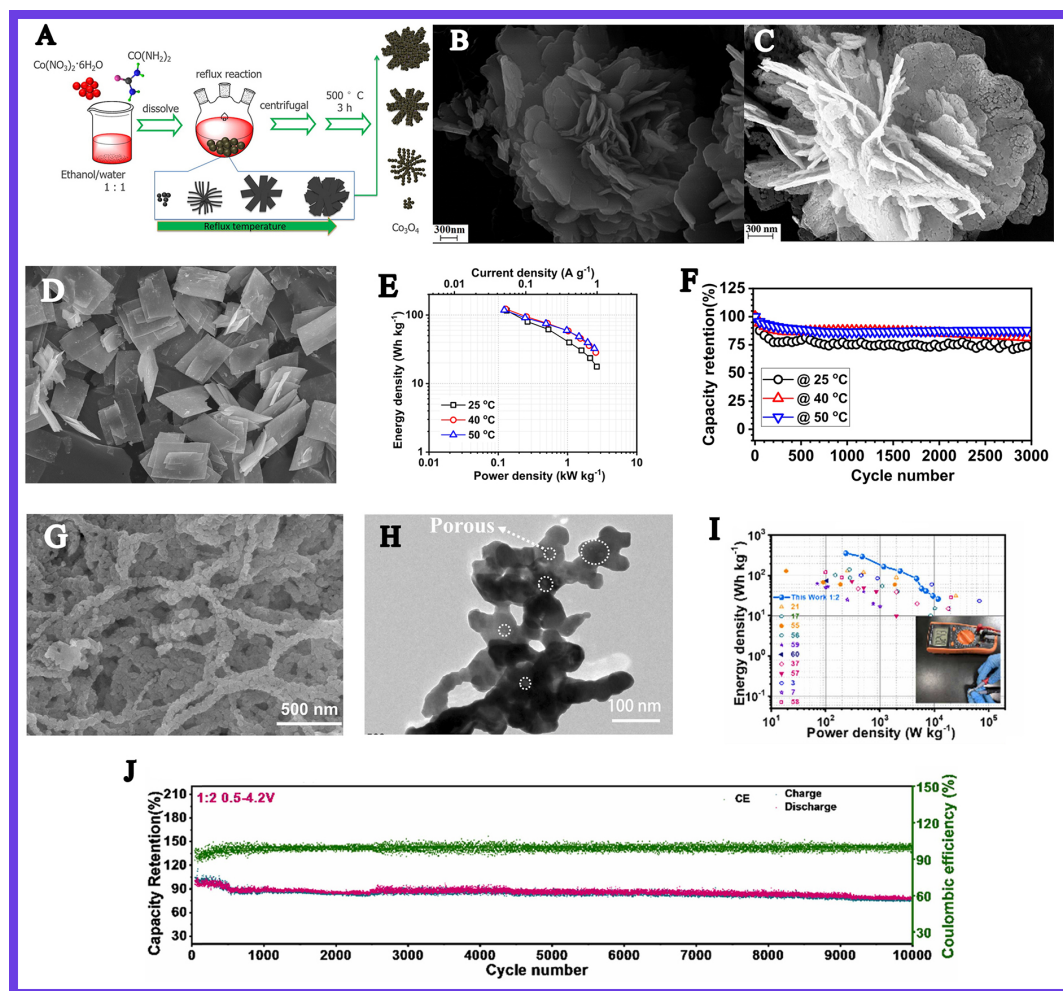


**Figure 6.** (A) Schematic preparation route for the Co-HLCs and Co<sub>3</sub>O<sub>4</sub>; SEM images of (B) Co-HLC-120 and (C) Co<sub>3</sub>O<sub>4</sub>-120. Reproduced with permission<sup>[172]</sup>. Copyright 2016, Elsevier B.V.; (D) SEM images of Co<sub>3</sub>O<sub>4</sub>-NSs; (E) Ragone plot of Co<sub>3</sub>O<sub>4</sub>-NSs//JFACs; (F) Cyclic stability of Co<sub>3</sub>O<sub>4</sub>-NSs//JFACs at different temperature. Reproduced with permission<sup>[173]</sup>. Copyright 2020, American Chemical Society; (G) The morphologies of NAC-L-Co<sub>3</sub>O<sub>4</sub> NFs; (H) TEM images of NAC-L-Co<sub>3</sub>O<sub>4</sub> NFs; (I) Ragone plots of the optimum NAC-L-Co<sub>3</sub>O<sub>4</sub>//NPCP LIC; (J) Cycling stability of the NAC-L-Co<sub>3</sub>O<sub>4</sub>//NPCP LIC. Reproduced with permission<sup>[174]</sup>. Copyright 2022, Elsevier B.V.

showed 796 mAh·g<sup>-1</sup> and even at 1.5 A·g<sup>-1</sup>, it can still deliver 648 mAh·g<sup>-1</sup>. Sennu *et al.* synthesized mesoporous 2D Co<sub>3</sub>O<sub>4</sub> nanosheets (Co<sub>3</sub>O<sub>4</sub>-NSs) through an elementary hydrothermal reaction [Figure 6D]<sup>[173]</sup>. And the Li/Co<sub>3</sub>O<sub>4</sub>-NS electrode delivered 2,270 mAh·g<sup>-1</sup> at 0.1 A·g<sup>-1</sup> between 0.05–3 V. And at 50 °C, the LICs employing Co<sub>3</sub>O<sub>4</sub>-NSs as LIBs-type components and Jack fruit derived activated carbons (JFACs) as electric double-layer capacitor (EDLC)-type electrodes displayed large ED of 118 Wh·kg<sup>-1</sup> at 125 W·kg<sup>-1</sup>, high PD of 2.6 kW·kg<sup>-1</sup> at 33 Wh·kg<sup>-1</sup>, and remarkable cycling stability with 87% capacity retention after 3,000 cycles at 0.2 A·g<sup>-1</sup> within 1.0–3.5 V [Figure 6E and F].

To further improve the electrical conductivity of Co<sub>3</sub>O<sub>4</sub>, Li *et al.* introduced nitrogen-doped amorphous carbon (NAC) to connect multi-porous Co<sub>3</sub>O<sub>4</sub> nanofibers, and synthesized NAC-L-Co<sub>3</sub>O<sub>4</sub> nanofiber films through electrospinning and annealing techniques<sup>[174]</sup>. The ability of NAC-L-Co<sub>3</sub>O<sub>4</sub> to maintain this nanofiber architecture post-pyrolysis is crucial because it suggests that the structural integrity and the elongated shape of the fibers are preserved. This is beneficial because nanofibers often provide a high

surface-to-volume ratio which is advantageous for various applications [Figure 6G and H]. Secondly, the emergence of nanosheets on the surface of these nanofibers is another critical structural characteristic observed after pyrolysis. Nanosheets are 2D structures with thickness in the nanometer scale. Their formation on the nanofibers of NAC<sub>L</sub>-Co<sub>3</sub>O<sub>4</sub> could be due to partial decomposition or reorganization of the material's surface during the high-temperature treatment. These nanosheets can significantly alter the surface properties of the nanofibers, potentially enhancing the material's performance in applications by increasing the available reactive surface area and modifying the electronic properties. The capacity of NAC<sub>L</sub>-Co<sub>3</sub>O<sub>4</sub> performed 1,200 mAh·g<sup>-1</sup> at 0.1 A·g<sup>-1</sup> within 0.01-3 V (vs. Li<sup>+</sup>/Li). When NAC<sub>L</sub>-Co<sub>3</sub>O<sub>4</sub> is used as the anode in LICs in combination with a nitrogen-doped porous carbon polyhedron (NPCP) cathode, the LICs have resulted in a remarkably high ED of 296 and 31.3 Wh·kg<sup>-1</sup> obtained at 470 W·kg<sup>-1</sup> and 9.4 kW·kg<sup>-1</sup>, spanning 0.5-4.2 V. Furthermore, the LICs exhibited remarkable cycling durability (80% after 10,000 cycles) when tested at 1 A·g<sup>-1</sup> [Figure 6I and J].

In addition to Co<sub>3</sub>O<sub>4</sub>, there are kinds of 2D TMOs that have great potential as negative electrode materials for LICs. MoO<sub>2</sub> is noted for having an exceptionally high conductivity of 104 S·cm<sup>-1</sup>. This level of conductivity is remarkably close to that of pure molybdenum metal, which stands at about 190 S·cm<sup>-1</sup>. High electrical conductivity in a material facilitates the rapid movement of electrons through the material, which is a critical attribute for any component used in electronics and ESDs. The high conductivity of MoO<sub>2</sub> means that when used in device applications, it can efficiently transport electrons, minimizing energy losses that occur due to resistance within the material, thereby enhancing the overall efficiency and performance of the device<sup>[175,176]</sup>. Additionally, MoO<sub>2</sub> is recognized for its excellent theoretical specific capacity. These two properties - high conductivity and excellent specific capacity - make MoO<sub>2</sub> a particularly potential material for use as an anode in LICs. Zhao *et al.* employed a one-step solvothermal reaction to create MoO<sub>2</sub> nanosheets<sup>[177]</sup>. The MoO<sub>2</sub> nanosheets produced through the aforementioned method exhibited variable levels of crystallinity. Enhancing Li<sup>+</sup> diffusion and promoting electron transport within this amorphous/crystalline hybrid structure imparts improved capacity and cycling performance to the resulting discrepant MoO<sub>2</sub> nanosheets. The TEM image in Figure 7A distinctly illustrates the ultra-thin nature of MoO<sub>2</sub>. Furthermore, the presence of amorphous MoO<sub>2</sub> regions is evident [Figure 7B]. The emergence of these amorphous regions results from the low synthesis temperature, which effectively inhibits the crystallization of MoO<sub>2</sub>. An as-prepared discrepant MoO<sub>2</sub> electrode (vs. Li<sup>+</sup>/Li) delivers 243 mAh·g<sup>-1</sup> at 0.1 A·g<sup>-1</sup> between 1.0-3.0 V. And the MoO<sub>2</sub>//AC LICs exhibited remarkable cycling stability over 4,000 cycles (85% at 5 A·g<sup>-1</sup>) and maximum ED and PD of 150 Wh·kg<sup>-1</sup> (at 163 W·kg<sup>-1</sup>) and 6.93 kW·kg<sup>-1</sup> (at 32 Wh·kg<sup>-1</sup>), spanning 1.5-4.2 V.

TiO<sub>2</sub> has been noticed as a potential electrode material for high-performance LIBs and LICs owing to its abundant availability, green and pollution-free, strong structural stability, remarkable ability for reversible lithiation and de-lithiation, and a safe operating voltage<sup>[180,181]</sup>. Liu *et al.* present a top-down approach to efficiently synthesize TiO<sub>2</sub> nanosheets with enhanced SSA, numerous pore structures, and TiO<sub>2</sub>-B/anatase heterointerfaces under mild conditions [Figure 7C]<sup>[178]</sup>. The performance characteristics of the engineered TiO<sub>2</sub> nanosheet material (denoted as SE-TONS) are particularly notable for their rapid Li<sup>+</sup> uptake and release capabilities, which are essential for enhancing the charging and discharging efficiency of LICs. This rapid ion exchange is crucial for applications requiring high power output and quick recharge times. Structurally, SE-TONS offers significant advantages due to its nanosheet configuration. This unique morphology significantly enlarges so more the contact area between the electrode and the electrolyte that the unique morphology of the electrode not only accommodates more active sites for ion attachment but also reduces the distance ions need to travel to enter or leave the electrode [Figure 7D-F]. Moreover, the compact arrangement within SE-TONS provides shorter transport pathways for Li<sup>+</sup> and electrons. This



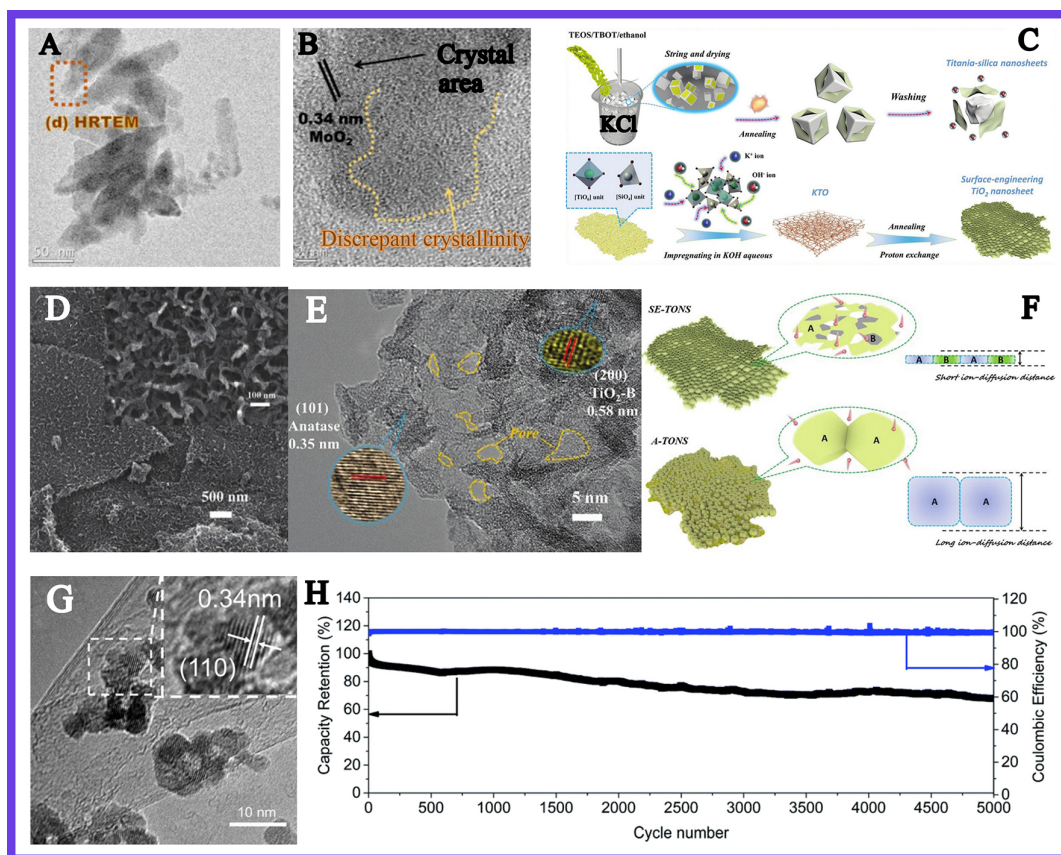


**Figure 7.** (A) TEM and (B) HRTEM of as-prepared discrepant MoO<sub>2</sub>. Reproduced with permission<sup>[177]</sup>. Copyright 2017, The Royal Society of Chemistry; (C) Schematic of the preparation of the SE-TONS sample; (D) SEM images of SE-TONS; (E) HR-TEM images of the SE-TONS sample; (F) Graphically illustration of the Li<sup>+</sup>-transport/storage behavior in the SE-TONS or A-TONS/electrolyte system. Reproduced with permission<sup>[178]</sup>. Copyright 2021, The Royal Society of Chemistry and the Chinese Chemical Society; (G) HRTEM images of SnO<sub>2</sub>/PCN; (H) Cycling performance of SnO<sub>2</sub>/PCNs//PCNs LIC. Reproduced with permission<sup>[179]</sup>. Copyright 2021, the Royal Society of Chemistry.

structural feature minimizes resistance and maximizes the speed of electrochemical reactions. Consequently, these attributes - enhanced contact area and reduced transport distances - collectively improve the performance of SE-TONS, making it an exceptional material choice for high-efficiency, fast-charging LICs. Specifically, it achieves 180 mAh·g<sup>-1</sup> at 0.5 A·g<sup>-1</sup> (1-3.0 V) and exhibits long-term stability by delivering 110 mAh·g<sup>-1</sup> over 1,000 cycles at 6 A·g<sup>-1</sup>. Additionally, when employed in a LIC with AC as a cathode, the SE-TONS//AC LICs delivered ED and PD of 61.5 Wh·kg<sup>-1</sup> (at 134 W·kg<sup>-1</sup>) and 5.5 kW·kg<sup>-1</sup> (at 40.2 Wh·kg<sup>-1</sup>), during 0.01-3.5 V, with a good capacity retention of 80% up to 10,000 cycles at 4.0 A·g<sup>-1</sup>.

Nevertheless, some of TMOs encounter several challenges that can impair their long-term performance and efficiency. One significant issue is their inherently low electrical conductivity, which can limit the speed of charge and discharge cycles and overall performance of the devices. Additionally, TMOs often undergo substantial volume changes during the charging and discharging processes. These volume fluctuations can be problematic, as they frequently lead to material pulverization and agglomeration. To mitigate these issues, a promising strategy involves the incorporation of a 2D carbon matrix within the TMO structure. This carbon matrix serves as a protective medium that not only enhances the overall conductivity of the electrode material but also helps to stabilize its structural changes. The flexibility and strength of the 2D carbon layers accommodate the volume expansions and contractions of TMOs during device operation,



effectively cushioning the material and preventing the severe impacts of pulverization and agglomeration. By doing so, this approach maintains the electrode's integrity and ensures a more stable and reliable performance over extended battery cycles<sup>[182]</sup>. Hence, integrating a 2D carbon matrix into TMOs presents a valuable solution to overcoming some of the key limitations these materials face in energy storage applications. Liu *et al.* showcase a straightforward method for constructing LICs using a porous carbon nanosheet (PCN) derived from waste coffee grounds as a cathode, and a composite anode composed of SnO<sub>2</sub> and PCNs [Figure 7G]<sup>[179]</sup>. And during 0.01–3.0 V vs. Li<sup>+</sup>/Li, SnO<sub>2</sub>/PCNs can deliver 2,225 mAh·g<sup>-1</sup> at 0.1 A·g<sup>-1</sup> and the capacity can be sustained at 313 mAh·g<sup>-1</sup> at 1 A·g<sup>-1</sup> after 500 cycles (nearly tenfold that of SnO<sub>2</sub>). The fabricated SnO<sub>2</sub>/PCNs//PCNs LICs achieved maximum ED of 138 Wh·kg<sup>-1</sup> at the PD of 416 W·kg<sup>-1</sup> and retained 51 Wh·kg<sup>-1</sup> at 53 kW·kg<sup>-1</sup>, with a capacitance retention of 67% after 5,000 cycles at 5 A·g<sup>-1</sup> from 1.0 to 4.0 V [Figure 7H].

The 2D TMOs are recognized for their high redox activity, a property that greatly enhances their performance in energy storage, particularly in applications involving intercalation reactions. The high redox activity of 2D TMOs facilitates these reactions effectively, allowing for the smooth accommodation of ions without causing significant structural changes to the material. This capability is crucial for maintaining the integrity and longevity of the devices during continuous cycles of charging and discharging. Additionally, the versatility of these materials in handling a diverse range of potential values adds to their utility in various electrochemical applications. The specific potential range that these oxides can operate within largely depends on the type of metallic centers incorporated within the oxides. These attributes render them appealing as electrode materials for LICs. However, challenges persist in harnessing 2D materials for the construction of high-performance LICs, such as preventing the restacking of nanosheets and addressing mechanical degradation, which can lead to inadequate electrolyte access and reduced cycling stability of the individual 2D material components. To surmount these limitations, one such approach is exploring new 2D architectures, which involves investigating and developing novel types of 2D structures. By diversifying the range of available 2D materials, researchers can tailor properties to better meet specific application needs. Another promising strategy is the intentional incorporation of defects into the atomic structure of these materials. Contrary to what might be expected, these defects can actually enhance the electrochemical properties of 2D materials by providing additional active sites for ion storage or improving ion transport pathways. Additionally, heterostructure engineering, which involves combining different materials in a layered structure, is proposed to improve functionality and overall performance. These heterostructures can exploit the complementary properties of different materials, thereby enhancing the electrochemical performance and stability of the resulting composite. Lastly, interlayer engineering, which focuses on modifying the interactions and spacing between layers in 2D materials, represents another frontier for improving their performance characteristics. By optimizing how these layers interact, it is possible to enhance the mechanical and electrochemical stability of the material, making it more suitable for high-capacity and high-durability energy storage applications.

### Transition-metal dichalcogenide

In 1923, 2D TMDs were initially discovered<sup>[183]</sup>. TMDs, characterized by the chemical formula MX<sub>2</sub> where “M” stands for a transition metal and “X” indicates a chalcogen (S, Se, or Te), exhibit a unique layered structure. Each unit features a plane of metal atoms sandwiched between two planes of chalcogen atoms, forming a distinct X-M-X arrangement<sup>[184–186]</sup>. This configuration is fundamentally two-dimensional, akin to graphene, but with a more complex, multilayered setup. The structure of TMDs contributes to several notable properties, including a large SSA and the quantum confinement effect, both of which are inherent to their 2D nature. These properties confer several advantages to TMDs in charge storage applications. The layered 2D structure enhances interface interactions with electrolytes, which is crucial for efficient charge transport. Additionally, the extensive surface area of TMD nanosheets increases the active points available

for electrochemical reactions. This feature, combined with the thin, flat nature of TMDs, significantly reduces the diffusion hindrance for electrolyte ions, thereby enhancing ionic mobility. Furthermore, the inherent structural integrity of TMDs helps to minimize volume changes during charge and discharge cycles, a critical factor for maintaining stability and durability in electrode materials<sup>[187,188]</sup>.

Nevertheless, it was not until 2017 that 2D TMDs were reported for use as electrode materials in LICs. The  $\text{TiS}_2$  crystal layer compound was synthesized by Chaturvedi *et al.* using chemical vapor transport technology (CVT)<sup>[189]</sup>. As shown in [Figure 8A](#) and [B](#), the synthesized  $\text{TiS}_2$  exhibits high purity and crystallinity, and features a triangular atomic arrangement. Between 1.5–2.8 V,  $\text{TiS}_2$  offered  $212 \text{ mAh}\cdot\text{g}^{-1}$  at  $0.1 \text{ A}\cdot\text{g}^{-1}$ . The LICs, fabricated by  $\text{TiS}_2$  as the anode with AC as the counter electrode, showed ED and PD of  $49 \text{ Wh}\cdot\text{kg}^{-1}$  at  $100 \text{ W}\cdot\text{kg}^{-1}$  and  $5.5 \text{ Wh}\cdot\text{kg}^{-1}$  at  $2.5 \text{ kW}\cdot\text{kg}^{-1}$ , as well as cycling performance with 76% capacity retention after 2,000 cycles at  $1 \text{ A}\cdot\text{g}^{-1}$  within 0.01–2.6 V. Similarly, Wang *et al.* successfully synthesized CoS nanosheets using a hydrothermal method, which is favored for crafting nanostructured materials<sup>[84]</sup>. These nanosheets are distinguished by their unique 3D hierarchical structure, reminiscent of walnut shapes, and are composed of interconnected hexagonal nanosheets with thicknesses ranging from 10 to 100 nm [[Figure 8C](#)]. This intricate structure not only prevents the aggregation or restacking of the nanosheets but also serves as a robust buffer reducing volume changes during the operation cycles, thus enhancing the structural stability of the electrode material. The structure facilitates stable capacity retention and enhanced ion diffusion. Specifically, the pores between the intercrossing nanosheets promote the diffusion of electrolytes, facilitating effective transmission of  $\text{Li}^+$ . This results in a high reversible capacity of  $434 \text{ mAh}\cdot\text{g}^{-1}$  at  $0.1 \text{ A}\cdot\text{g}^{-1}$ , demonstrating excellent lithium storage stability within 1.0 to 3.0 V vs.  $\text{Li}^+/\text{Li}$ . Moreover, these nanosheets were utilized in a novel LIC device, where the CoS anode was paired with a biochar-based cathode derived from fructus cannabis shells (FCS), exhibiting ideal EDLC behavior. This CoS//FCS LIC achieved an impressive maximum ED of  $125.2 \text{ Wh}\cdot\text{kg}^{-1}$  at a PD of  $160 \text{ W}\cdot\text{kg}^{-1}$ , while maintaining  $60.8 \text{ Wh}\cdot\text{kg}^{-1}$  at an elevated PD of  $6,400 \text{ W}\cdot\text{kg}^{-1}$ . Additionally, the device exhibited exceptional cycle life with capacitance retention of 81.75% after 40,000 cycles at  $1 \text{ A}\cdot\text{g}^{-1}$  from 1.0 to 4.2 V.

While individual TMDs have exhibited satisfactory performance, researchers are continually seeking enhanced capabilities. Given the distinct characteristics of different materials, the combination of materials with complementary properties holds the promise of achieving superior performance.  $\text{MoS}_2$ , a representative 2D TMD, is regarded as a promising electrode due to its layered S-Mo-S sandwich structure and abundant ion storage sites. The 1T- $\text{MoS}_2$  variant, characterized by enhanced conductivity and a larger inter-layer space compared to 2H- $\text{MoS}_2$ , facilitates rapid  $\text{Li}^+$  storage. However, pristine  $\text{MoS}_2$  often experiences significant volume changes during charge and discharge processes, adversely affecting electrochemical performance. The construction of hybrids has proven to be an effective strategy to address this issue<sup>[191,192]</sup>. Ju *et al.* successfully prepared porous carbon nanofibers/ $\text{MoS}_2$  nanosheet-flower ball composites (3D-PCNF/ $\text{MoS}_2$ -NFFBs) using 3D porous carbon nanofibers as carriers by a hydrothermal method<sup>[193]</sup>. At a  $0.05 \text{ A}\cdot\text{g}^{-1}$  (during 0.01–3 V vs.  $\text{Li}^+/\text{Li}$ ); it showed  $749.54 \text{ mAh}\cdot\text{g}^{-1}$ , and even at  $2 \text{ A}\cdot\text{g}^{-1}$ , 3D-PCNF/ $\text{MoS}_2$ -NFFBs can still deliver  $428.57 \text{ mAh}\cdot\text{g}^{-1}$ . The outcomes were attributed to the uniform dispersion of  $\text{MoS}_2$ , the establishment of a conductive pathway by the PCNF skeleton, and the presence of numerous mesopores within the 3D-PCNF/ $\text{MoS}_2$ -NFFBs. These factors collectively increased the reaction area, minimized paths for  $\text{Li}^+$  diffusion, mitigated volume expansion, and accelerated electron transfer. In addition, the 3D-PCNF/ $\text{MoS}_2$ -NFFBs//AC LICs showed excellent ED ( $75.5 \text{ Wh}\cdot\text{kg}^{-1}$  at  $75 \text{ W}\cdot\text{kg}^{-1}$ ), ultra PD ( $30 \text{ kW}\cdot\text{kg}^{-1}$  at  $22.5 \text{ Wh}\cdot\text{kg}^{-1}$ ) and 78% capacity retention after 5,000 cycles at  $1 \text{ A}\cdot\text{g}^{-1}$ , during 0.01–3.0 V. Liu *et al.* synthesized nitrogen-doped graphene-coated flower-like  $\text{MoS}_2$  nanosheets (FL- $\text{MoS}_2$ /N-G) using the polyacrylamide (PAM)-assisted method [[Figure 8D](#)]<sup>[190]</sup>. The attachment of PAM to the (002) plane of  $\text{MoS}_2$  represents a significant advancement in modifying the surface properties of this 2D material. By

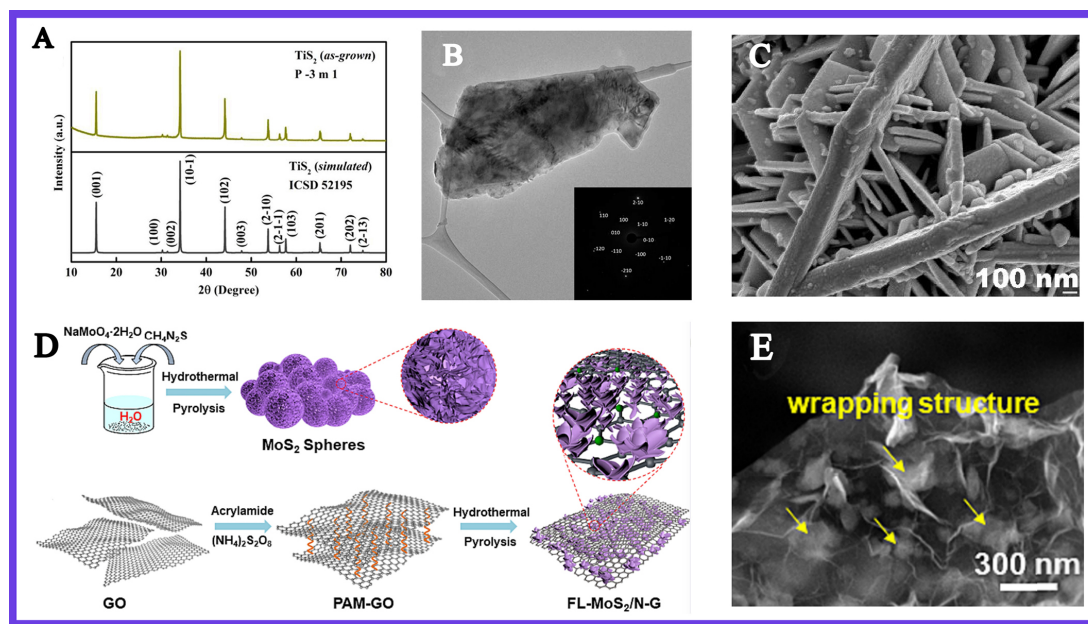


**Figure 8.** (A) Semi-quantitative analysis of as-grown  $\text{TiS}_2$  crystallites; (B) Ragone of the  $\text{TiS}_2//\text{AC}$  LICs. Reproduced with permission<sup>[189]</sup>. Copyright 2017, The Royal Society of Chemistry; (C) SEM images for CoS. Reproduced with permission<sup>[84]</sup>. Copyright 2019, American Chemical Society; (D) Schematic illustration for the fabrication of  $\text{MoS}_2$  and FL- $\text{MoS}_2/\text{N-G}$ ; (E) SEM images of FL- $\text{MoS}_2/\text{N-G}$  samples. Reproduced with permission<sup>[190]</sup>. Copyright 2023, Elsevier B.V.

attaching PAM, the surface energy of  $\text{MoS}_2$  is notably reduced, which directly influences the behavior and stability of the nanosheets. This decreased surface energy is crucial because it helps to prevent the common issue of re-stacking or agglomeration among nanosheets. Furthermore, the interaction between PAM and  $\text{MoS}_2$  does more than just stabilize the nanosheets; it also induces a specific structural organization. The presence of PAM encourages the  $\text{MoS}_2$  nanosheets to orient radially, leading to a distinctive and functional structural formation. As a result of this radial orientation, the nanosheets naturally assemble into a flower-like structure, which is not only aesthetically appealing but also beneficial for applications that require a high surface area and specific morphological properties. This structurally organized assembly enhances the functional characteristics of the  $\text{MoS}_2$ , making it more effective in its applications by providing a larger and more accessible reactive surface area and preventing the loss of functionality due to agglomeration [Figure 8E]. By combining  $\text{MoS}_2$  nanosheets with nitrogen-doped graphene, the composite material facilitates a faster movement of electrical charges, which is crucial for improving the efficiency and responsiveness of electronic devices and batteries. Moreover, the integrated structure of  $\text{MoS}_2$  nanosheets and nitrogen-doped graphene not only enhances electrical conductivity but also creates additional sites for  $\text{Li}^+$  storage. This increase in available lithium storage sites directly contributes to the enhanced lithium storage capacity of the material, making it highly beneficial for applications in LICs where higher energy densities are desired. Additionally, the coupling significantly reduces the diffusion resistance encountered by  $\text{Li}^+$  within the material. By decreasing this resistance, the ionic conductivity of the material is improved, resulting in faster ion transport. This reduction in diffusion resistance is particularly important in high-performance ESSs, where rapid ion movement is essential for high power delivery and quick recharging capabilities. Within 0.01–3 V vs.  $\text{Li}^+/\text{Li}$ , the as-prepared FL- $\text{MoS}_2/\text{N-G}$  delivered 1,152  $\text{mAh}\cdot\text{g}^{-1}$  at 0.1  $\text{A}\cdot\text{g}^{-1}$ . Impressively, The FL- $\text{MoS}_2/\text{N-G}/\text{AC}$  LICs displayed large ED of 111.6  $\text{Wh}\cdot\text{kg}^{-1}$  at 200  $\text{W}\cdot\text{kg}^{-1}$ , high PD of 40  $\text{kW}\cdot\text{kg}^{-1}$  at 61.6  $\text{Wh}\cdot\text{kg}^{-1}$ , and cycling stability with 87% capacity retention after 10,000 cycles at 5  $\text{A}\cdot\text{g}^{-1}$  within 0.01–4.0 V.

Numerous compounds within the TMD family have undergone scrutiny for lithium storage. Nevertheless, the exploration of TMDs specifically as electrode materials for LICs is still evolving. Given the exceptional electrochemical performance demonstrated by TMDs in lithium storage applications, the future development of TMDs-based electrode materials for LICs hinges significantly on a rational design and appropriate structural considerations.

### MXenes

In recent years, MXene materials, as a newly discovered family of 2D materials, have garnered attention in academic research, which exhibit a rich variety of surface functional groups that can be employed to modulate surface redox reactions<sup>[194]</sup>. With a large interlayer spacing allowing for enhanced ion accommodation and high conductivity, MXene materials present extensive application prospects, particularly in the field of electrochemical energy storage, sparking a surge in research interest. When employed as electrodes in LICs, the metallic conductivity and layered structure of MXene offer additional chemical activity interfaces and a reduced ion diffusion length. Consequently, MXene proves effective in mitigating imbalances in ion dynamics between the anode and cathode<sup>[195-198]</sup>. As far back as 2012, Naguib *et al.* identified that the  $\text{Li}^+$  charge storage in  $\text{Ti}_2\text{C}$  MXene resulted from  $\text{Li}^+$  intercalation, as opposed to a conversion reaction<sup>[199]</sup>. Furthermore, Come *et al.* obtained  $\text{Ti}_2\text{C}$  by exfoliating  $\text{Ti}_2\text{AlC}$ , and within 0.05-2.7 V vs.  $\text{Li}^+/\text{Li}$ , the as-prepared  $\text{Ti}_2\text{C}$  delivered 172  $\text{mAh}\cdot\text{g}^{-1}$  at 0.025  $\text{A}\cdot\text{g}^{-1}$ <sup>[200]</sup>. Impressively, the  $\text{Ti}_2\text{C}/\text{AC}$  LICs displayed an ED of 50  $\text{Wh}\cdot\text{kg}^{-1}$ , high PD of 190  $\text{kW}\cdot\text{kg}^{-1}$  and cycling stability with 85.7% capacity retention after 1,000 cycles at 2.5  $\text{A}\cdot\text{g}^{-1}$  within 1.0-3.5 V. MXenes, as electrodes in LICs, present potential advantages due to their enhanced electrochemical performance when compared to traditional graphite electrodes. This improvement is attributed to the distinctive attributes of MXenes which include high conductivity and flexibility. However, MXenes face a significant challenge: their initially narrow interlayer spacing. This can impede the diffusion and storage of  $\text{Li}^+$ , which is critical for the efficiency of ESDs. To address these limitations, researchers are actively pursuing various strategies. These include the development of novel MXene variants and the modification of the type and concentration of terminal groups on the surface of MXenes. Another critical strategy is interlayer engineering, which involves adjusting the interlayer spacing to enhance the storage capabilities of MXenes. This is achieved by leveraging the weak van der Waals forces between the layers, allowing for a more flexible approach to structural modifications. The benefits of interlayer engineering are particularly notable. By increasing the interlayer space, the capacity for  $\text{Li}^+$  to intercalate within the MXene structure can be significantly enhanced. This improvement in intercalation capability translates directly to better energy storage performance, as it allows for more efficient ion transport and accommodation within the electrode material.

$\text{Ti}_3\text{C}_2\text{T}_x$ , a representative of MXene family, has undergone extensive study, with diverse intercalating agents experimented upon to augment its interlayer spacing and consequently modify its characteristics. Guo *et al.* prepared  $\text{VN}/\text{Ti}_3\text{C}_2\text{T}_x$  composites [Figure 9A] by vacuum filtration method<sup>[201]</sup>. VN nanowires serve as “spacers” between MXene nanosheets to prevent restacking, thereby increasing the interlayer spacing [Figure 9B]. This facilitates unobstructed pathways for electrolyte ions, enhancing rate capability and capacity. Between 0.01-3.0 V,  $\text{VN}/\text{Ti}_3\text{C}_2\text{T}_x$  offered 501.7  $\text{mAh}\cdot\text{g}^{-1}$  at 0.1  $\text{A}\cdot\text{g}^{-1}$  and 191.8  $\text{mAh}\cdot\text{g}^{-1}$  even at 5  $\text{A}\cdot\text{g}^{-1}$ , which showed a better outstanding rate performance. The PD of  $\text{VN}/\text{Ti}_3\text{C}_2\text{T}_x$ /egg white-derived AC (E-AC) LIC device is 449.7  $\text{W}\cdot\text{kg}^{-1}$  when ED is 129.3  $\text{Wh}\cdot\text{kg}^{-1}$ ; besides, ED for the device remains at 42.81  $\text{Wh}\cdot\text{kg}^{-1}$  when the PD is 11.249  $\text{kW}\cdot\text{kg}^{-1}$ . In addition, the device capacitance retention is 98.3% after cycling 5,000 at 1  $\text{A}\cdot\text{g}^{-1}$  from 0.5-4.0 V.

Wang *et al.* developed a novel heterostructure by combining 1T- $\text{MoS}_2$  nanosheets with delaminated  $\text{Ti}_3\text{C}_2\text{T}_x$  MXene<sup>[86]</sup>, using tetrabutylammonium hydroxide (TBAOH) in the fabrication process [Figure 9C]. This method effectively facilitated the dispersion of MXene, which is essential for achieving uniform material



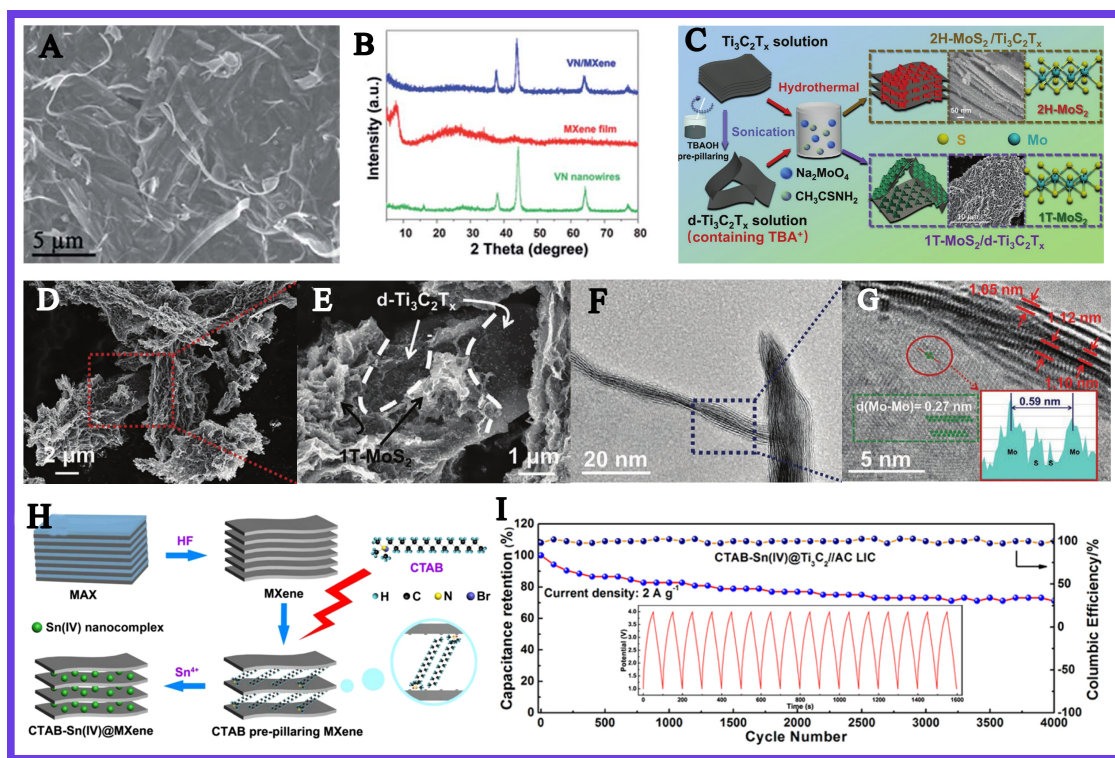


**Figure 9.** (A) SEM images of VN/ $\text{Ti}_3\text{C}_2\text{T}_x$  composite; (B) XRD patterns of the  $\text{Ti}_3\text{C}_2\text{T}_x$  film, VN nanowires and VN/ $\text{Ti}_3\text{C}_2\text{T}_x$  composite, respectively. Reproduced with permission<sup>[201]</sup>. Copyright 2022, the Royal Society of Chemistry; (C) Schematic illustration of the fabrication process of 1T- $\text{MoS}_2$ / $\text{d-Ti}_3\text{C}_2\text{T}_x$  heterostructure; (D and E) SEM images of the dividing line between the different components in 1T- $\text{MoS}_2$ / $\text{d-Ti}_3\text{C}_2\text{T}_x$ ; (F and G) HRTEM images of 1T- $\text{MoS}_2$ / $\text{d-Ti}_3\text{C}_2\text{T}_x$ . Reproduced with permission<sup>[86]</sup>. Copyright 2021, Wiley-VCH; (H) Schematic illustration of preparation of CTAB-Sn(IV)@ $\text{Ti}_3\text{C}_2$ ; (I) Long-term cycling performance of CTAB-Sn(IV)@ $\text{Ti}_3\text{C}_2$ //AC LIC. Reproduced with permission<sup>[87]</sup>. Copyright 2016, American Chemical Society.

properties across various applications. Moreover, it enabled the vertical arrangement of 1T- $\text{MoS}_2$  on the  $\text{Ti}_3\text{C}_2\text{T}_x$  surface, a type of MXene. This vertical arrangement is particularly beneficial as it can optimize the exposure of active sites and enhance the electrochemical interactions necessary in energy storage applications. A key component of this methodology involves the use of TBA<sup>+</sup> ions. These ions play a crucial role as they trigger a phase transition in  $\text{MoS}_2$  from the semiconducting 2H phase to the more conductive metallic 1T phase. This transition is not merely a change in electrical properties but also involves significant structural changes. Specifically, the phase transition is accompanied by an expansion of the interlayer distance in  $\text{MoS}_2$  to over 1 nm. This expansion during the hydrothermal reaction process is particularly advantageous as it enhances the electrochemical properties of the material [Figure 9D-G]. The electrochemical performance of the resulting 1T- $\text{MoS}_2$ / $\text{d-Ti}_3\text{C}_2\text{T}_x$  heterostructure was remarkable, achieving 1,160  $\text{mAh}\cdot\text{g}^{-1}$  at 0.25  $\text{A}\cdot\text{g}^{-1}$ , within 0.01 to 3.0 V (vs. Li<sup>+</sup>/Li). When this heterostructure was utilized as the anode material in LICs, paired with a hierarchically structured graphene nanocomposite (GNC) cathode, the devices showcased exceptionally high ED. Specifically, they achieved an ED of 188  $\text{Wh}\cdot\text{kg}^{-1}$  at a PD of 168  $\text{W}\cdot\text{kg}^{-1}$ , and 22  $\text{Wh}\cdot\text{kg}^{-1}$  at a PD of 13  $\text{kW}\cdot\text{kg}^{-1}$ , across 0.1 to 4.0 V. Moreover, the LICs exhibited outstanding cycling durability, retaining 84.2% of their initial capacity after 1,000 cycles at 2  $\text{A}\cdot\text{g}^{-1}$ . In addition, Luo *et al.* employed a liquid-phase method utilizing cetyltrimethylammonium bromide (CTAB) for initial pre-pillaring, followed by the incorporation of Sn<sup>2+</sup> to further enhance the structure<sup>[87]</sup>, resulting in the formation of CTAB-Sn(IV)@ $\text{Ti}_3\text{C}_2$  [Figure 9H]. This method significantly increased the interlayer distance of the MXene to 2.708 nm, marking a 177% increase from the original spacing. Such structural enhancement was crucial in facilitating greater ion diffusion rates and storage capacities. Electrochemically,



CTAB-Sn(IV)@Ti<sub>3</sub>C<sub>2</sub> demonstrated 765 mAh·g<sup>-1</sup> at 0.1 A·g<sup>-1</sup>, which significantly outperformed other variants such as Sn(IV)@Ti<sub>3</sub>C<sub>2</sub> and CTAB@Ti<sub>3</sub>C<sub>2</sub>. When used as an anode material in LIC configurations, paired with an AC cathode, the resulting LICs delivered an impressive ED of 105.56 Wh·kg<sup>-1</sup> at a PD of 495 W·kg<sup>-1</sup>, and maintained 45.31 Wh·kg<sup>-1</sup> at a high PD of 10.8 kW·kg<sup>-1</sup>. Additionally, these capacitors showcased long-term cycling stability, retaining 71.1% of their capacity after 4,000 cycles at 2.0 A·g<sup>-1</sup> [Figure 9I].

## CONCLUSIONS AND PERSPECTIVE

The comprehensive review presented in the text offers a detailed overview of recent advancements in the application of 2D materials for anode use in LICs, including a detailed comparison and evaluation of these materials [Tables 1 and 2], which are crucial for high-energy and high-power applications. The adoption of graphene and other 2D materials has notably improved the rate performance and stability of anodes, which is crucial for developing LICs that demand high performance. Furthermore, the successful integration of these advanced 2D materials into LICs has enabled the achievement of high ED, high PD, and prolonged cycle life, marking substantial progress in the field.

Despite the intrinsic unique properties of 2D materials, such as high surface area and electrical conductivity, their practical integration into LICs has yet to deliver optimal results. This unsatisfactory performance signals a clear need for improvements if LICs using 2D materials are to achieve levels suitable for real-world demands. To bridge this performance gap, specific challenges associated with the integration of 2D materials into LICs must be identified and effectively addressed.

Firstly, the advancement of electrode materials stands as a pivotal aspect of energy storage technology, with an emphasis on the exploration and refinement of pseudocapacitive materials known for their impressive high capacity and swift rate capabilities. The strategic modification of these materials at the nanoscale level, through careful adjustment of their nanostructure and chemical composition, coupled with the innovative assembly of 2D nanosheets into 3D porous frameworks, holds the promise of significantly bolstering the functional efficacy of electrode materials. Such enhancements could pave the way for electrodes that exhibit superior performance metrics, capable of meeting the demanding requirements of modern ESSs.

Secondly, the large-scale production of 2D materials is not just a manufacturing challenge but a cornerstone for their integration into LICs. To harness the full potential of these materials in commercial applications, it is imperative to establish synthesis processes that not only scale up production but also meticulously control the quality of the materials produced. Consistency in the properties of 2D materials is paramount to ensure reliability and efficiency in their use, making the development of such controlled synthesis methods a research priority.

Thirdly, a notable challenge in the deployment of 2D materials, and by extension their assembled 3D architectures, is their typically low gravimetric density, which can be a significant hurdle in practical applications. To overcome this, it is essential to strike a delicate balance between the porosity of the materials - to ensure ionic accessibility and surface area - and their mass density - to maximize volumetric ED. Developing suitable electrode configurations that can reconcile these opposing factors is crucial for the realization of high-performance ESDs that are both powerful and practical.

Fourthly, the issue of irreversible capacity loss during initial charging cycles, a common shortcoming in lithium-ion storage technologies, calls for the development of convenient and effective pre-lithiation strategies. Such methods would compensate for the initial capacity loss and ensure that the full capacity of

**Table 1. The electrochemical characteristics and challenges of different 2D anode materials**

<b>Graphene</b>	Energy storage mechanism	Graphene stores Li <sup>+</sup> through intercalation between its layers. The optimal interlayer spacing (0.77-0.83 nm) facilitates efficient Li <sup>+</sup> intercalation, potentially enhancing the capacity up to 744 mAh·g <sup>-1</sup>
	Electrochemical properties	Graphene exhibits high specific capacity, excellent rate capability, and good cycling stability. However, the formation of SEI can consume Li <sup>+</sup> and reduce the overall capacity. Pre-lithiation processes can mitigate this issue and improve the initial capacity
	Challenges	The lithium intercalation potential of graphene (0.1-0.5 V) is higher than that of graphite, which reduces the ED of LICs. Improving the graphitization degree and exploring new graphene materials are necessary to lower the lithium insertion potential and achieve high-rate performance
<b>TMOs</b>	Energy storage mechanism	TMOs store Li <sup>+</sup> through a conversion reaction mechanism. The transition metal is reduced and forms Li <sub>2</sub> O during lithiation, resulting in high specific capacity but also causing volume changes
	Electrochemical properties	TMOs demonstrate high specific capacity and good rate capability. However, the conversion reaction can lead to poor cycling stability and voltage hysteresis, affecting the overall performance
	Challenges	Addressing the volume changes and improving the cycling stability are the main challenges for TMOs. Nanostructuring, compositing with conductive additives, and surface modification are being investigated to mitigate these issues and enhance the electrochemical performance
<b>TMDs</b>	Energy storage mechanism	TMDs store Li <sup>+</sup> through a conversion reaction mechanism, where the transition metal is reduced and forms Li <sub>2</sub> S or Li <sub>2</sub> Se. This mechanism enables high specific capacity but can cause volume changes and structural instability
	Electrochemical properties	TMDs exhibit high specific capacity and good rate capability. However, the conversion reaction can lead to poor cycling stability due to the volume changes and structural degradation during repeated lithiation/delithiation processes
	Challenges	Improving the cycling stability of TMDs is a major challenge. Strategies such as nanostructuring, compositing with conductive matrices, and surface modification are being explored to mitigate the volume changes and enhance the structural stability
<b>MXenes</b>	Energy storage mechanism	MXenes store Li <sup>+</sup> through a combination of intercalation and surface redox reactions. The unique 2D layered structure and surface functional groups of MXenes facilitate fast Li <sup>+</sup> transport and provide abundant active sites for storage
	Electrochemical properties	MXenes demonstrate high specific capacity, excellent rate capability, and good cycling stability. The presence of surface functional groups enhances the pseudocapacitive contribution, leading to improved electrochemical performance
	Challenges	The restacking of MXenes nanosheets during synthesis and electrode fabrication can limit the accessible surface area and hinder Li <sup>+</sup> transport. Strategies such as interlayer engineering and compositing with conductive additives are needed to address this issue

the electrode materials is available for use in practical applications. The design of pre-lithiation techniques that are both user-friendly and highly efficient would represent a significant advancement in prolonging the lifespan and usability of lithium-ion-based devices.

Finally, the exploration of novel electrode configurations is essential to mitigate the prevalent issues of electrode kinetics and capacity imbalances. Innovative concepts such as the “dual carbon” configuration, where both the anode and cathode are carbon-based, offer a symmetrical approach that can potentially improve the overall kinetics and cycling stability of the device. Similarly, the “pseudo-capacitor” configuration, which leverages the fast charge-discharge capabilities of pseudocapacitive materials, could address capacity disparities. The investigation into these and other novel electrode designs is likely to yield configurations that are not only efficient and balanced but also conducive to the next generation of energy storage solutions.

**Table 2. The electrochemical performance of 2D materials for LICs anode**

Anode	Cathode	Voltage (V)	Max energy density (Wh·kg <sup>-1</sup> ) @power density (W·kg <sup>-1</sup> )	Max power density (W·kg <sup>-1</sup> ) @energy density (Wh·kg <sup>-1</sup> )	Cycling stability	Reference
Pre-lithiated graphene	AC	~	98.1@18	222.2@67	0.4 A·g <sup>-1</sup> , 74% after 300 cycles	[105]
SG-1000	HPC-10	2.0-4.2	131@57	6,323@37	5 A·g <sup>-1</sup> , 89.1% after 10,000 cycles	[106]
SHSG	NHCN	2-4.5	146@650	103@52	4 A·g <sup>-1</sup> , 91% after 40,000 cycles	[108]
NMG	NMG	0.01-4.0	128@500	10,000@92	4 A·g <sup>-1</sup> , 98.3% after 4,000 cycles	[81]
rGO800-P	AC	1.5-4.5	91@145	26,000@33	5 A·g <sup>-1</sup> , 76% after 10,000 cycles	[82]
NPG	AC	1.0-4.0	195@746.2	14,983.7@77	1 A·g <sup>-1</sup> , 94.2% after 5,000 cycles	[83]
OMG-2	OMG-2	0.01-4.0	131.6@2,272	21,660@87.3	4 A·g <sup>-1</sup> , 96.8% after 5,000 cycles	[137]
CoSe <sub>2</sub> /N-rGO	AC	1.0-4.2	104.2@270.6	5,452.7@84.9	1 A·g <sup>-1</sup> , 81.2% after 8,000 cycles	[89]
R-TNO	AC	0-3.0	142.1@375	18,750@81	4 A·g <sup>-1</sup> , 88% after 10,000 cycles	[48]
rGO/MnO	AC	1-4.4	194.6@269.3	40,700@57.4	2 A·g <sup>-1</sup> , 77.9% after 10,000 cycles	[90]
Co <sub>3</sub> O <sub>4</sub> -NSs	JFACs	1.0-3.5	118@125	2,600@33	0.2 A·g <sup>-1</sup> , 87% after 3,000 cycles	[173]
NAC <sub>L</sub> -Co <sub>3</sub> O <sub>4</sub>	NPCP	0.5-4.2	296@470	9,400@31.3	1 A·g <sup>-1</sup> , 80% after 10,000 cycles	[174]
MoO <sub>2</sub>	AC	1.5-4.2	150@163	6,930@32	5 A·g <sup>-1</sup> , 85% after 4,000 cycles	[177]
SE-TONS	AC	0.01-3.5	61.5@134	5,500@40.2	4 A·g <sup>-1</sup> , 80% after 10,000 cycles	[178]
SnO <sub>2</sub> /PCNs	PCNs	1.0-4.0	138@416	53,000@51	5 A·g <sup>-1</sup> , 67% after 5,000 cycles	[179]
TiS <sub>2</sub>	AC	0.01-2.6	49@100	2,500@5.5	1 A·g <sup>-1</sup> , 76% after 2,000 cycles	[189]
CoS	FCS	1.0-4.2	125.2@160	6,400@60.8	1 A·g <sup>-1</sup> , 81.75% after 40,000 cycles	[84]
3D-PCNF/MoS <sub>2</sub> -NFFBs	AC	0.01-3.0	75.5@75	30,000@22.5	1 A·g <sup>-1</sup> , 78% after 5,000 cycles	[193]
FL-MoS <sub>2</sub> /N-G	AC	0.01-4.0	111.6@200	40,000@61.6	5 A·g <sup>-1</sup> , 87% after 10,000 cycles	[190]
VN/Ti <sub>3</sub> C <sub>2</sub> T <sub>x</sub>	E-AC	0.5-4.0	129.3@449.7	11,249@42.81	1 A·g <sup>-1</sup> , 98.3% after 5,000 cycles	[201]
1T-MoS <sub>2</sub> /d-Ti <sub>3</sub> C <sub>2</sub> T <sub>x</sub>	GNC	0.1-4.0	188@168	13,000@22	2 A·g <sup>-1</sup> , 84.2% after 1,000 cycles	[86]
CTAB-Sn(IV)@Ti <sub>3</sub> C <sub>2</sub>	AC	1.0-4.0	105.56@495	10,800@45.31	2 A·g <sup>-1</sup> , 71.1% after 4,000 cycles	[87]

## DECLARATIONS

### Authors' contributions

Conceptualization, investigation, and writing of original draft: Hu T, Zhang X, Li C

Formal analysis: An Y, Zhao S, Sun X, Wang K

Supervision and writing of review and editing: Zhang X, Ma Y

**Availability of data and materials**

Not applicable.

**Financial support and sponsorship**

Not applicable.

**Conflicts of interest**

All authors declared that there are no conflicts of interest.

**Ethical approval and consent to participate**

Not applicable.

**Consent for publication**

Not applicable.

**Copyright**

© The Author(s) 2024.

**REFERENCES**

1. Sathish S, Kumaravelu TA, Yang C, et al. Enhancing supercapacitor performance with biomass-derived activated carbon interlinked CoS<sub>2</sub> embedded graphitic carbon nitride. *J Alloy Compd* 2024;985:174076. DOI
2. Wu W, Diwu J, Guo J, et al. Hierarchical architecture of ZIF-8@ZIF-67-derived N-doped carbon nanotube hollow polyhedron supported on 2D Ti<sub>3</sub>C<sub>2</sub>T<sub>x</sub> nanosheets targeting enhanced lithium-ion capacitors. *J Colloid Interface Sci* 2024;663:609-23. DOI
3. Yuan X, Jiang T, Tay CY, He Y, Wang H, Zhang G. Magnetization roasting combined with multi-stage extraction for selective recovery of lithium from spent lithium-ion batteries. *Sep Purif Technol* 2024;338:126349. DOI
4. Yang L, Chen J, Park S, Wang H. Recent progress on metal-organic framework derived carbon and their composites as anode materials for potassium-ion batteries. *Energy Mater* 2023;3:300042. DOI
5. Deng XG, Fan LQ, Fu XY, et al. Carbon-reinforced Ni<sub>3</sub>S<sub>2</sub>/Ti<sub>3</sub>C<sub>2</sub>T<sub>x</sub> MXene composite as an anode for superior-performance lithium-ion capacitors. *J Colloid Interface Sci* 2024;661:237-48. DOI
6. Sun PP, Deng SP, Li JQ, et al. A MOF-derived flower-shaped CeCo-oxide as a multifunctional material for high-performance lithium-ion batteries and supercapacitors. *J Colloid Interface Sci* 2024;661:564-73. DOI
7. Ge Q, Ma Z, Yao M, et al. Carbon-coated tin-titanate derived SnO<sub>2</sub>/TiO<sub>2</sub> nanowires as high-performance anode for lithium-ion batteries. *J Colloid Interface Sci* 2024;661:888-96. DOI
8. Gao X, Zhang S, Guo J, Zhang H, Li S, Zhang Z. Surface structure regulation toward anionic redox activation of Li<sub>1.20</sub>Mn<sub>0.533</sub>Ni<sub>0.133</sub>Co<sub>0.133</sub>O<sub>2</sub> cathodes with high initial coulombic efficiency. *J Colloid Interface Sci* 2024;663:601-8. DOI
9. Yu H, Liu J, Wu X, Li R, Jin R, Zhou G. Construction of mesocrystal Cu<sub>2-x</sub>Se nanoplates with high infiltration for enhanced electrochemical performance in lithium ion batteries and electrochemical supercapacitors. *Appl Surf Sci* 2024;655:159530. DOI
10. Yu H, Li Y, Liu F, Wang L, Song Y. Yolk shell structured YS-Si@N-doped carbon derived from covalent organic frameworks for enhanced lithium storage. *J Colloid Interface Sci* 2024;662:313-21. DOI
11. Zhao L, Zhong Y, Cao C, Tang T, Shao Z. Enhanced high-temperature cycling stability of garnet-based all solid-state lithium battery using a multi-functional catholyte buffer layer. *Nanomicro Lett* 2024;16:124. DOI PubMed PMC
12. Sun G, Zhuang S, Jiang S, et al. Dual-modified surface encapsulation strategy for elevating rate performance and cycling stability of Ni-rich NCM811 cathode. *J Energy Stor* 2024;84:110821. DOI
13. Tharani S, Prithiba A. Sustainable biomass conversion into activated carbon for supercapacitor devices: a promising approach toward renewable energy storage. *Energy Sour Part A* 2024;46:1165-76. DOI
14. Lu C, Yu Z, Zhang X, Ma X. ZnCl<sub>2</sub>-KOH modulation of biomass-derived porous carbon for supercapacitors. *Energy Sour Part A* 2024;46:2212-22. DOI
15. Yoshino A. The lithium-ion battery: two breakthroughs in development and two reasons for the Nobel prize. *Bull Chem Soc Jpn* 2022;95:195-7. DOI
16. Wang D, Jiang H, Feng M, Wang L, Yin D, Cheng Y. A universal multifunctional rare earth oxide coating strategy to stabilize high-nickel lithium layered oxide cathode. *J Alloy Compd* 2024;976:173364. DOI
17. Li Z, Han M, Yu P, Lin J, Yu J. Macroporous directed and interconnected carbon architectures endow amorphous silicon nanodots as low-strain and fast-charging anode for lithium-ion batteries. *Nanomicro Lett* 2024;16:98. DOI PubMed PMC
18. Kong Y, Yuan L, Liao Y, Shao Y, Hao S, Huang Y. Efficient separation and selective Li recycling of spent LiFePO<sub>4</sub> cathode. *Energy Mater* 2023;3:300053. DOI



19. Khan AU, Tahir K, Almarhoon ZM, et al. A new binder-free ZnS-CuO microsphere: a battery-type electrode material for asymmetric supercapacitor. *J Energy Stor* 2024;80:110308. DOI
20. Mo B, Wang L, Li L, et al. Supercapacitor performances of coal tar pitch based spherical active carbons fabricated by the SiO<sub>2</sub> template method. *J Chem Eng Jpn* 2023;56:2217863. DOI
21. Zhou W, Liu Z, Chen W, et al. A review on thermal behaviors and thermal management systems for supercapacitors. *Batteries* 2023;9:128. DOI
22. Li C, Zhang X, Lv Z, et al. Scalable combustion synthesis of graphene-welded activated carbon for high-performance supercapacitors. *Chem Eng J* 2021;414:128781. DOI
23. Li C, Zhang X, Wang K, et al. Recent advances in carbon nanostructures prepared from carbon dioxide for high-performance supercapacitors. *J Energy Chem* 2021;54:352-67. DOI
24. Pang L, Hoang MT, O'Mullane AP, Wang H. Revealing energy storage mechanism of CsPbBr<sub>3</sub> perovskite for ultra-stable symmetric supercapacitors. *Energy Mater* 2023;3:300012. DOI
25. Zhong C, Weng S, Wang Z, Zhan C, Wang X. Kinetic limits and enhancement of graphite anode for fast-charging lithium-ion batteries. *Nano Energy* 2023;117:108894. DOI
26. Zheng S, Yu S, Ullah Z, et al.  $\pi$ -d conjugation regulates the cathode/electrolyte interface in all-solid-state lithium-ion batteries. *J Mater Chem A* 2024;12:3967-76. DOI
27. Niu L, Wu T, Chen M, et al. Conductive metal-organic frameworks for supercapacitors. *Adv Mater* 2022;34:e2200999. DOI
28. Amatucci GG, Badway F, Du Pasquier A, Zheng T. An asymmetric hybrid nonaqueous energy storage cell. *J Electrochem Soc* 2001;148:A930. DOI
29. Jagadale A, Zhou X, Xiong R, Dubal DP, Xu J, Yang S. Lithium ion capacitors (LICs): development of the materials. *Energy Stor Mater* 2019;19:314-29. DOI
30. Naoi K, Ishimoto S, Miyamoto J, Naoi W. Second generation 'nanohybrid supercapacitor': evolution of capacitive energy storage devices. *Energy Environ Sci* 2012;5:9363-73. DOI
31. Zhang X, Sun X, An Y, et al. Design of a fast-charge lithium-ion capacitor pack for automated guided vehicle. *J Energy Stor* 2022;48:104045. DOI
32. Zhou W, Liu Z, An Y, et al. Thermal behavior analysis of lithium-ion capacitors at transient high discharge rates. *J Energy Stor* 2022;53:105208. DOI
33. An Y, Li C, Sun X, et al. Deoxygenated porous carbon with highly stable electrochemical reaction interface for practical high-performance lithium-ion capacitors. *J Phys D Appl Phys* 2022;55:045501. DOI
34. Guo Z, Liu Z, Sun X, et al. Probing current contribution of lithium-ion battery/lithium-ion capacitor multi-structure hybrid systems. *J Power Sources* 2022;548:232016. DOI
35. Wang P, Sun X, An Y, et al. Additives to propylene carbonate-based electrolytes for lithium-ion capacitors. *Rare Met* 2022;41:1304-13. DOI
36. Li C, Zhang X, Wang K, Sun X, Ma Y. High-power lithium-ion hybrid supercapacitor enabled by holey carbon nanolayers with targeted porosity. *J Power Sources* 2018;400:468-77. DOI
37. Jiao A, Gao J, He Z, Hou J, Kong L. Perovskite fluoride NaNiF<sub>3</sub> with hollow micron sphere structure as anode for Li-ion hybrid capacitors. *Rare Met* 2022;41:3370-80. DOI
38. Jiao A, Duan Y, Li Z, Zhang S, Su T, Fu Z. Nanostructured octahedral MnF<sub>2</sub> as anode material for constructing ultra-high power Li-ion hybrid capacitors. *Electrochim Acta* 2024;475:143595. DOI
39. Duan Y, Li Z, Zhang S, et al. Metal-organic frameworks (MOFs)-derived Mn<sub>2</sub>SnO<sub>4</sub>@C anode based on dual lithium storage mechanism for high-performance lithium-ion capacitors. *Chem Eng J* 2023;477:146914. DOI
40. Zhao C, Niu D, Liu T, et al. Hierarchical electrode constructed by carbon-coated metal-organic framework derivatives supported on two-dimensional Ti<sub>3</sub>C<sub>2</sub> nanosheets for hybrid Li-ion capacitors. *J Taiwan Inst Chem Eng* 2024;155:105290. DOI
41. Yang F, Zhang Z, Li H, et al. Construction of anode materials for NiSe-based high energy density lithium-ion capacitors. *Mater Today Commun* 2024;38:107816. DOI
42. Zhou W, Liu Z, Chen W, et al. Thermal characteristics of pouch lithium-ion battery capacitors based on activated carbon and LiNi<sub>1/3</sub>Co<sub>1/3</sub>Mn<sub>1/3</sub>O<sub>2</sub>. *J Energy Stor* 2023;66:107474. DOI
43. Song S, Zhang X, An Y, et al. Floating aging mechanism of lithium-ion capacitors: impedance model and post-mortem analysis. *J Power Sources* 2023;557:232597. DOI
44. Sun X, Zhang X, Wang K, et al. Determination strategy of stable electrochemical operating voltage window for practical lithium-ion capacitors. *Electrochim Acta* 2022;428:140972. DOI
45. Song S, Zhang X, An Y, Ma Y. Advanced fractional-order lithium-ion capacitor model with time-domain parameter identification method. *IEEE Trans Ind Electron* 2022;69:13808-17. DOI
46. Zhang J, Chen Z, Xu T, et al. Vanadium nitride nanoparticles embedded in carbon matrix with pseudocapacitive behavior for high performance lithium-ion capacitors. *Rare Met* 2022;41:2460-9. DOI
47. Jin L, Yuan J, Shellikeri A, et al. An overview on design parameters of practical lithium-ion capacitors. *Batteries Supercaps* 2021;4:749-57. DOI
48. Chaturvedi P, Lokhande A, Managutti P, Choi D. Free-standing TiNb<sub>6</sub>O<sub>17</sub>/rGO composites as a superior anode host for high-performance Li-ion capacitor. *J Alloy Compd* 2024;971:172739. DOI

49. Huang X, Zhang C, Chen M, Yang Y.  $\text{Li}_2\text{C}_2\text{O}_4$  with 3D confinement as simultaneous sacrificial material and activation reagent of biomass-derived carbon for advanced lithium-ion capacitors. *Mater Today Sustain* 2023;24:100567. DOI
50. Choi JW, Park DG, Kim KH, Choi WH, Park MG, Kang JK. 3D nitrogen-doped carbon frameworks with hierarchical pores and graphitic carbon channels for high-performance hybrid energy storages. *Mater Horiz* 2024;11:566-77. DOI PubMed
51. Akshay M, Jyothilakshmi S, Lee YS, Aravindan V. High-performance Li-ion and Na-ion capacitors based on a spinel  $\text{Li}_4\text{Ti}_5\text{O}_{12}$  anode and carbonaceous cathodes. *Small* 2024;20:e2307248. DOI PubMed
52. Li C, An Y, Wang L, et al. Balancing microcrystalline domains in hard carbon with robust kinetics for a  $46.7 \text{ Wh kg}^{-1}$  practical lithium-ion capacitor. *Chem Eng J* 2024;485:149880. DOI
53. Sun X, An Y, Zhang X, et al. Unveil Overcharge performances of activated carbon cathode in various Li-ion electrolytes. *Batteries* 2023;9:11. DOI
54. Liu F, Lu P, Zhang Y, et al. Sustainable lignin-derived carbon as capacity-kinetics matched cathode and anode towards 4.5 V high-performance lithium-ion capacitors. *Energy Environ Mater* 2023;6:e12550. DOI
55. Ma Y, Li S, An Y, et al. A practical high-energy lithium-ion capacitor enabled by multiple conducting bridges triggered electrode current reallocation. *Energy Stor Mater* 2023;62:102946. DOI
56. Peng Q, Wang K, Gong Y, et al. Tailoring lignin-derived porous carbon toward high-energy lithium-ion capacitor through varying  $\text{Sp}^2$ - and  $\text{Sp}^3$ -hybridized bonding. *Adv Funct Mater* 2023;33:2308284. DOI
57. Sun C, Zhang X, Li C, et al. A safe, low-cost and high-efficiency presodiation strategy for pouch-type sodium-ion capacitors with high energy density. *J Energy Chem* 2022;64:442-50. DOI
58. Jin L, Gong R, Zhang W, et al. Toward high energy-density and long cycling-lifespan lithium ion capacitors: a 3D carbon modified low-potential  $\text{Li}_2\text{TiSiO}_5$  anode coupled with a lignin-derived activated carbon cathode. *J Mater Chem A* 2019;7:8234-44. DOI
59. Guo Z, Liu Z, Chen W, et al. Battery-type lithium-ion hybrid capacitors: current status and future perspectives. *Batteries* 2023;9:74. DOI
60. Li X, Hou Y, Yin Z, Xiang S, Yin C, Yin Z. High mass-loading N-rGO-T- $\text{Nb}_2\text{O}_5$ /CuNW composite membrane for high-rate lithium-ion capacitor anodes. *J Energy Stor* 2023;73:109003. DOI
61. Zhang X, Zhang K, Zhang W, et al. Carbon nano-onion-encapsulated Ni nanoparticles for high-performance lithium-ion capacitors. *Batteries* 2023;9:102. DOI
62. Cheng C, Wu D, Gong T, et al. Internal and external cultivation design of zero-strain columbite-structured  $\text{MNb}_2\text{O}_6$  toward lithium-ion capacitors as competitive anodes. *Adv Energy Mater* 2023;13:2302107. DOI
63. Novoselov KS, Geim AK, Morozov SV, et al. Electric field effect in atomically thin carbon films. *Science* 2004;306:666-9. DOI
64. Khan R, Andreescu S. Catalytic  $\text{MXCeO}_2$  for enzyme based electrochemical biosensors: fabrication, characterization and application towards a wearable sweat biosensor. *Biosens Bioelectron* 2024;248:115975. DOI PubMed
65. Ali SR, Praveen C, Kang SG, Nair L, Bhamu K, Kumar P. Exploring the catalytic properties of  $\text{Ti}_2\text{CO}_2$  MXene decorated with Cu-cluster for hydrogen evolution reaction. *Appl Surf Sci* 2023;641:158439. DOI
66. Xu Z, Zhang K, Li Y, Zhang Y, Zhao X, Wang Y. Synthesis of SiC nanowires wrapped in trimetallic layered double hydroxide nanosheets with core-shell structure via self-assembly growth approach for effective electromagnetic wave absorption. *J Alloy Compd* 2024;976:173316. DOI
67. Zeng L, Tang T, Liang Y, Jiang S, Xu X, Wang F. Molybdate-intercalated NiMn layered double hydroxide nanoarrays supercapacitor electrode with enhanced stability via a differentiated deposition strategy. *J Power Sources* 2024;594:233990. DOI
68. Khan J, Ahmad RTM, Yu Q, Liu H, Khan U, Liu B. A  $\text{La}_2\text{O}_3$ /MXene composite electrode for supercapacitors with improved capacitance and cycling performance. *Sci Technol Adv Mater* 2023;24:2242262. DOI PubMed PMC
69. Chatterjee S, Gawas R, Snyder J. Top-down electrochemical synthesis of nanoporous metal nanosheets from nonlayered alloy precursors. *Adv Eng Mater* 2024;26:2301538. DOI
70. Zhao Z, Yang J, Wang C, et al. Template-free synthesis of highly porous silica-doped alumina with exceptional stability via intercalation-exfoliation of boehmite into two-dimensional nanosheets. *Sci China Mater* 2024;67:261-71. DOI
71. Li X, Hajinur Hirad A, Alarfaj AA, Li H, Santhanam R. A convergent fabrication of graphene oxide/silk fibroin/hydroxyapatite nanocomposites delivery improved early osteoblast cell adhesion and bone regeneration. *Arab J Chem* 2024;17:105468. DOI
72. Wazir N, Li Y, Ullah R, et al. Enhancing growth of high-quality two-dimensional  $\text{CsPbBr}_3$  flakes on sapphire substrate by direct chemical vapor deposition method. *FlatChem* 2024;43:100598. DOI
73. Hu Y, Rogée L, Wang W, et al. Extendable piezo/ferroelectricity in nonstoichiometric 2D transition metal dichalcogenides. *Nat Commun* 2023;14:8470. DOI PubMed PMC
74. Wu Y, Yang J, Zheng M, et al. Two-dimensional cobalt ferrite through direct chemical vapor deposition for efficient oxygen evolution reaction. *Chinese J Catal* 2023;55:265-77. DOI
75. Papavasileiou AV, Antonatos N, Luxa J, et al. Two-dimensional  $\text{VSe}_2$  nanoflakes as a promising sensing electrocatalyst for nitrobenzene determination in water samples. *Electrochim Acta* 2024;475:143653. DOI
76. Xin X, Zhao B, Yue J, et al. A universal strategy for producing 2D functional carbon-rich materials from 2D porous organic polymers for dual-carbon lithium-ion capacitors. *New Carbon Mater* 2023;38:898-912. DOI
77. Zhang S, Fang R, Zhang L, Huang S, Zhao Y, Wang Y. Fully coated  $\text{WS}_2$  antioxidant film with mesoporous structure for enhancing the structural stability and CDI performance of MXene. *Desalination* 2024;574:117226. DOI
78. T.E. S, Tran DT, Jena S, et al. Flexible 2D borophene-stacked MXene heterostructure for high-performance supercapacitors. *Chem*

- Eng J* 2024;481:148266. DOI
79. Qin J, Yang Z, Xing F, Zhang L, Zhang H, Wu Z. Two-dimensional mesoporous materials for energy storage and conversion: current status, chemical synthesis and challenging perspectives. *Electrochem Energy Rev* 2023;6:9. DOI
  80. Tian LL, Wei XY, Zhuang QC, et al. Bottom-up synthesis of nitrogen-doped graphene sheets for ultrafast lithium storage. *Nanoscale* 2014;6:6075-83. DOI
  81. Ma X, Yu Z, Zhao L, et al. N-doped mesoporous graphene with superior capacitive behaviors derived from chemical vapor deposition methodology in the fluidized bed reactor. *Ind Eng Chem Res* 2018;57:16327-34. DOI
  82. Moreno-Fernández G, Granados-moreno M, Gómez-urbano JL, Carriazo D. Phosphorus-functionalized graphene for lithium-ion capacitors with improved power and cyclability. *Batteries Supercaps* 2021;4:469-78. DOI
  83. Luan Y, Hu R, Fang Y, et al. Nitrogen and phosphorus dual-doped multilayer graphene as universal anode for full carbon-based lithium and potassium ion capacitors. *Nanomicro Lett* 2019;11:30. DOI PubMed PMC
  84. Wang YK, Liu MC, Cao J, et al. 3D hierarchically structured CoS nanosheets: Li<sup>+</sup> storage mechanism and application of the high-performance lithium-ion capacitors. *ACS Appl Mater Interfaces* 2020;12:3709-18. DOI
  85. Yoo E, Kim J, Hosono E, Zhou HS, Kudo T, Honma I. Large reversible Li storage of graphene nanosheet families for use in rechargeable lithium ion batteries. *Nano Lett* 2008;8:2277-82. DOI PubMed
  86. Wang L, Zhang X, Xu Y, et al. Tetrabutylammonium-intercalated 1T-MoS<sub>2</sub> nanosheets with expanded interlayer spacing vertically coupled on 2D delaminated MXene for high-performance lithium-ion capacitors. *Adv Funct Mater* 2021;31:2104286. DOI
  87. Luo J, Zhang W, Yuan H, et al. Pillared structure design of MXene with ultralarge interlayer spacing for high-performance lithium-ion capacitors. *ACS Nano* 2017;11:2459-69. DOI
  88. Bo Z, Zheng Z, Huang Y, et al. One-step MXene selenization-conversion into carbon-scaffold-anchored TiSe<sub>2</sub> nanosheets enabling interlayer- and vacancy-mediated ion transport mechanisms for fast lithium-ion storage. *Chem Eng J* 2023;473:145183. DOI
  89. Wei W, Wang L, Liang C, et al. Interface engineering of CoSe<sub>2</sub>/N-doped graphene heterostructure with ultrafast pseudocapacitive kinetics for high-performance lithium-ion capacitors. *Chem Eng J* 2023;474:145788. DOI
  90. Liu W, Zhang X, Xu Y, et al. 2D graphene/MnO heterostructure with strongly stable interface enabling high-performance flexible solid-state lithium-ion capacitors. *Adv Funct Mater* 2022;32:2202342. DOI
  91. Tao S, Cai J, Cao Z, et al. Revealing the valence evolution of metal element in heterostructures for ultra-high power Li-ion capacitors. *Adv Energy Mater* 2023;13:2301653. DOI
  92. Tao S, Momen R, Luo Z, et al. Trapping lithium selenides with evolving heterogeneous interfaces for high-power lithium-ion capacitors. *Small* 2023;19:e2207975. DOI
  93. Huang H, Li Z, Gu S, et al. Dextran sulfate lithium as versatile binder to stabilize high-voltage LiCoO<sub>2</sub> to 4.6 V. *Adv Energy Mater* 2021;11:2101864. DOI
  94. Wang Y, Zhang Q, Xue Z, et al. An in situ formed surface coating layer enabling LiCoO<sub>2</sub> with stable 4.6 V high-voltage cycle performances. *Adv Energy Mater* 2020;10:2001413. DOI
  95. Su F, Hou X, Qin J, Wu Z. Recent advances and challenges of two-dimensional materials for high-energy and high-power lithium-ion capacitors. *Batteries Supercaps* 2020;3:10-29. DOI
  96. Tomy M, Ambika Rajappan A, Vm V, Thankappan Suryabai X. Emergence of novel 2D materials for high-performance supercapacitor electrode applications: a brief review. *Energy Fuels* 2021;35:19881-900. DOI
  97. Forouzandeh P, Pillai SC. Two-dimensional (2D) electrode materials for supercapacitors. *Mater Today Proc* 2021;41:498-505. DOI
  98. Billot N, Beyer M, Koch N, Ihle C, Reinhart G. Development of an adhesion model for graphite-based lithium-ion battery anodes. *J Manuf Syst* 2021;58:131-42. DOI
  99. Che Y, Lin X, Xing L, et al. Protective electrode/electrolyte interphases for high energy lithium-ion batteries with p-toluenesulfonyl fluoride electrolyte additive. *J Energy Chem* 2021;52:361-71. DOI
  100. Zhou H, Zhu S, Hibino M, Honma I, Ichihara M. Lithium storage in ordered mesoporous carbon (CMK-3) with high reversible specific energy capacity and good cycling performance. *Adv Mater* 2003;15:2107-11. DOI
  101. Suzuki T, Hasegawa T, Mukai SR, Tamon H. A theoretical study on storage states of Li ions in carbon anodes of Li ion batteries using molecular orbital calculations. *Carbon* 2003;41:1933-9. DOI
  102. Liang M, Luo B, Zhi L. Application of graphene and graphene-based materials in clean energy-related devices. *Int J Energy Res* 2009;33:1161-70. DOI
  103. Li D, Müller MB, Gilje S, Kaner RB, Wallace GG. Processable aqueous dispersions of graphene nanosheets. *Nat Nanotechnol* 2008;3:101-5. DOI PubMed
  104. Liu W, An Y, Wang L, et al. Mechanically flexible reduced graphene oxide/carbon composite films for high-performance quasi-solid-state lithium-ion capacitors. *J Energy Chem* 2023;80:68-76. DOI
  105. Ren J, Su L, Qin X, et al. Pre-lithiated graphene nanosheets as negative electrode materials for Li-ion capacitors with high power and energy density. *J Power Sources* 2014;264:108-13. DOI
  106. Wang J, Yan Z, Yan G, et al. Spiral graphene coupling hierarchically porous carbon advances dual-carbon lithium ion capacitor. *Energy Stor Mater* 2021;38:528-34. DOI
  107. Li C, Zhang X, Wang K, et al. Scalable self-propagating high-temperature synthesis of graphene for supercapacitors with superior power density and cyclic stability. *Adv Mater* 2017;29:1604690. DOI
  108. Li C, Zhang X, Wang K, Sun X, Ma Y. High-power and long-life lithium-ion capacitors constructed from N-doped hierarchical

- carbon nanolayer cathode and mesoporous graphene anode. *Carbon* 2018;140:237-48. DOI
109. Han S, Wu D, Li S, Zhang F, Feng X. Porous graphene materials for advanced electrochemical energy storage and conversion devices. *Adv Mater* 2014;26:849-64. DOI
110. Raccichini R, Varzi A, Passerini S, Scrosati B. The role of graphene for electrochemical energy storage. *Nat Mater* 2015;14:271-9. DOI PubMed
111. Ma Y, Wang K, Xu Y, et al. Dehalogenation produces graphene wrapped carbon cages as fast-kinetics and large-capacity anode for lithium-ion capacitors. *Carbon* 2023;202:175-85. DOI
112. Jin L, Guo X, Gong R, et al. Target-oriented electrode constructions toward ultra-fast and ultra-stable all-graphene lithium ion capacitors. *Energy Stor Mater* 2019;23:409-17. DOI
113. Ding J, Hu W, Paek E, Mitlin D. Review of hybrid ion capacitors: from aqueous to lithium to sodium. *Chem Rev* 2018;118:6457-98. DOI PubMed
114. Li B, Zheng J, Zhang H, et al. Electrode materials, electrolytes, and challenges in nonaqueous lithium-ion capacitors. *Adv Mater* 2018;30:e1705670. DOI
115. Sun C, Zhang X, An Y, et al. Molecularly chemical prelithiation of soft carbon towards high-performance lithium-ion capacitors. *J Energy Stor* 2022;56:106009. DOI
116. Sun C, Zhang X, Li C, Wang K, Sun X, Ma Y. High-efficiency sacrificial prelithiation of lithium-ion capacitors with superior energy-storage performance. *Energy Stor Mater* 2020;24:160-6. DOI
117. Sun C, Zhang X, Li C, Wang K, Sun X, Ma Y. Recent advances in prelithiation materials and approaches for lithium-ion batteries and capacitors. *Energy Stor Mater* 2020;32:497-516. DOI
118. Jiang J, Li Z, Zhang Z, et al. Recent advances and perspectives on prelithiation strategies for lithium-ion capacitors. *Rare Met* 2022;41:3322-35. DOI
119. Jin L, Shen C, Shellikeri A, et al. Progress and perspectives on pre-lithiation technologies for lithium ion capacitors. *Energy Environ Sci* 2020;13:2341-62. DOI
120. Li G, Yang Z, Yin Z, et al. Non-aqueous dual-carbon lithium-ion capacitors: a review. *J Mater Chem A* 2019;7:15541-63. DOI
121. Kang HJ, Huh YS, Im WB, Jun YS. Molecular cooperative assembly-mediated synthesis of ultra-high-performance hard carbon anodes for dual-carbon sodium hybrid capacitors. *ACS Nano* 2019;13:11935-46. DOI PubMed
122. Pollak E, Geng B, Jeon KJ, et al. The interaction of  $\text{Li}^+$  with single-layer and few-layer graphene. *Nano Lett* 2010;10:3386-8. DOI
123. Ferre-Vilaplana A. Storage of hydrogen adsorbed on alkali metal doped single-layer all-carbon materials. *J Phys Chem C* 2008;112:3998-4004. DOI
124. Yao F, Güneş F, Ta HQ, et al. Diffusion mechanism of lithium ion through basal plane of layered graphene. *J Am Chem Soc* 2012;134:8646-54. DOI
125. Ma X, Gao D. High capacitive storage performance of sulfur and nitrogen codoped mesoporous graphene. *ChemSusChem* 2018;11:1048-55. DOI PubMed
126. Wu ZS, Ren W, Xu L, Li F, Cheng HM. Doped graphene sheets as anode materials with superhigh rate and large capacity for lithium ion batteries. *ACS Nano* 2011;5:5463-71. DOI
127. Mao Y, Duan H, Xu B, et al. Lithium storage in nitrogen-rich mesoporous carbon materials. *Energy Environ Sci* 2012;5:7950-5. DOI
128. Jin Z, Yao J, Kittrell C, Tour JM. Large-scale growth and characterizations of nitrogen-doped monolayer graphene sheets. *ACS Nano* 2011;5:4112-7. DOI PubMed
129. Li X, Geng D, Zhang Y, Meng X, Li R, Sun X. Superior cycle stability of nitrogen-doped graphene nanosheets as anodes for lithium ion batteries. *Electrochem Commun* 2011;13:822-5. DOI
130. Wang H, Zhang C, Liu Z, et al. Nitrogen-doped graphene nanosheets with excellent lithium storage properties. *J Mater Chem* 2011;21:5430. DOI
131. Sun C, Zhang X, An Y, et al. Low-temperature carbonized nitrogen-doped hard carbon nanofiber toward high-performance sodium-ion capacitors. *Energy Environ Mater* 2023;6:e12603. DOI
132. Wang L, Zhang X, Kong Y, et al. Metal-organic framework-derived  $\text{CoSe}_2$ @N-doped carbon nanocubes for high-performance lithium-ion capacitors. *Rare Met* 2024;43:2150-60. DOI
133. Li T, Huang X, Lei S, et al. Two-dimensional nitrogen and phosphorus co-doped mesoporous carbon-graphene nanosheets anode for high-performance potassium-ion capacitor. *Energy Mater* 2023;3:300018. DOI
134. Yan T, Wen F, Duan J, et al. Fabricating tunable metal sulfides embedded with honeycomb-structured N-doped carbon matrices for high-performance lithium-ion capacitors. *Chem Eng J* 2023;474:145839. DOI
135. Ma C, Shao X, Cao D. Nitrogen-doped graphene nanosheets as anode materials for lithium ion batteries: a first-principles study. *J Mater Chem* 2012;22:8911-5. DOI
136. Kong XK, Chen QW. Improved performance of graphene doped with pyridinic N for Li-ion battery: a density functional theory model. *Phys Chem Chem Phys* 2013;15:12982-7. DOI PubMed
137. Xiao Z, Zhao L, Yu Z, et al. Multilayered graphene endowing superior dispersibility for excellent low temperature performance in lithium-ion capacitor as both anode and cathode. *Chem Eng J* 2022;429:132358. DOI
138. Xia Q, Yang H, Wang M, et al. High energy and high power lithium-ion capacitors based on boron and nitrogen dual-doped 3D carbon nanofibers as both cathode and anode. *Adv Energy Mater* 2017;7:1701336. DOI
139. Li Z, Bommier C, Chong ZS, et al. Mechanism of Na-ion storage in hard carbon anodes revealed by heteroatom doping. *Adv Energy*



- Mater* 2017;7:1602894. DOI
140. Zhang C, Mahmood N, Yin H, Liu F, Hou Y. Synthesis of phosphorus-doped graphene and its multifunctional applications for oxygen reduction reaction and lithium ion batteries. *Adv Mater* 2013;25:4932-7. DOI PubMed
  141. Ma C, Deng C, Liao X, He Y, Ma Z, Xiong H. Nitrogen and phosphorus codoped porous carbon framework as anode material for high rate lithium-ion batteries. *ACS Appl Mater Interfaces* 2018;10:36969-75. DOI PubMed
  142. Ghosh S, Barg S, Jeong SM, Ostrikov K. Heteroatom-doped and oxygen-functionalized nanocarbons for high-performance supercapacitors. *Adv Energy Mater* 2020;10:2001239. DOI
  143. Chen Z, Cao R, Ge Y, Tu Y, Xia Y, Yang X. N- and O-doped hollow carbonaceous spheres with hierarchical porous structure for potential application in high-performance capacitance. *J Power Sources* 2017;363:356-64. DOI
  144. Olabi A, Abdelkareem MA, Wilberforce T, Sayed ET. Application of graphene in energy storage device - a review. *Renew Sustain Energy Rev* 2021;135:110026. DOI
  145. Liang H, Li X, Zheng W, et al. Rational design of heterostructured core-shell Co-Zn bimetallic selenides for improved sodium-ion storage. *Rare Met* 2022;41:3381-90. DOI
  146. Aghamohammadi H, Hassanzadeh N, Eslami-farsani R. A review study on titanium niobium oxide-based composite anodes for Li-ion batteries: synthesis, structure, and performance. *Ceram Int* 2021;47:26598-619. DOI
  147. Wang H, Qian R, Cheng Y, et al. Micro/nanostructured TiNb<sub>2</sub>O<sub>7</sub>-related electrode materials for high-performance electrochemical energy storage: recent advances and future prospects. *J Mater Chem A* 2020;8:18425-63. DOI
  148. Lin C, Wang G, Lin S, Li J, Lu L. TiNb<sub>6</sub>O<sub>17</sub>: a new electrode material for lithium-ion batteries. *Chem Commun* 2015;51:8970-3. DOI
  149. Mao W, Bao K, Wang L, et al. Synthesis of TiNb<sub>6</sub>O<sub>17</sub>/C composite with enhanced rate capability for lithium ion batteries. *Ceram Int* 2016;42:16935-40. DOI
  150. Shang Y, Lu S, Zheng W, et al. Facile synthesis of carbon and oxygen vacancy co-modified TiNb<sub>6</sub>O<sub>17</sub> as an anode material for lithium-ion batteries. *RSC Adv* 2022;12:13127-34. DOI PubMed PMC
  151. Yuan Y, Yu H, Cheng X, et al. Preparation of TiNb<sub>6</sub>O<sub>17</sub> nanospheres as high-performance anode candidates for lithium-ion storage. *Chem Eng J* 2019;374:937-46. DOI
  152. Zhu G, Wang L, Lin H, et al. Walnut-like multicore-shell MnO encapsulated nitrogen-rich carbon nanocapsules as anode material for long-cycling and soft-packed lithium-ion batteries. *Adv Funct Mater* 2018;28:1800003. DOI
  153. Xiao Y, Xu C, Wang P, et al. Encapsulating MnO nanoparticles within foam-like carbon nanosheet matrix for fast and durable lithium storage. *Nano Energy* 2018;50:675-84. DOI
  154. An C, Li Y, Wu S, et al. Matched MnO@C anode and porous carbon cathode for Li-ion hybrid supercapacitors. *Rare Met* 2023;42:1959-68. DOI
  155. Lin J, Zeng C, Lin X, Xu C, Xu X, Luo Y. Metal-organic framework-derived hierarchical MnO/Co with oxygen vacancies toward elevated-temperature Li-ion battery. *ACS Nano* 2021;15:4594-607. DOI PubMed
  156. Chu Y, Guo L, Xi B, et al. Embedding MnO@Mn<sub>3</sub>O<sub>4</sub> nanoparticles in an N-doped-carbon framework derived from Mn-organic clusters for efficient lithium storage. *Adv Mater* 2018;30:1704244. DOI
  157. Cai Z, Xu L, Yan M, et al. Manganese oxide/carbon yolk-shell nanorod anodes for high capacity lithium batteries. *Nano Lett* 2015;15:738-44. DOI
  158. Yi S, Wang L, Zhang X, et al. Cationic intermediates assisted self-assembly two-dimensional Ti<sub>3</sub>C<sub>2</sub>T<sub>x</sub>/rGO hybrid nanoflakes for advanced lithium-ion capacitors. *Sci Bull* 2021;66:914-24. DOI
  159. Guo J, Wang R, Tjiu WW, Pan J, Liu T. Synthesis of Fe nanoparticles@graphene composites for environmental applications. *J Hazard Mater* 2012;225-6:63-73. DOI PubMed
  160. Liang S, Zhang S, Liu Z, et al. Approaching the theoretical sodium storage capacity and ultrahigh rate of layer-expanded MoS<sub>2</sub> by interfacial engineering on N-doped graphene. *Adv Energy Mater* 2021;11:2002600. DOI
  161. Chen P, Zhou W, Xiao Z, et al. In situ anchoring MnO nanoparticles on self-supported 3D interconnected graphene scroll framework: a fast kinetics boosted ultrahigh-rate anode for Li-ion capacitor. *Energy Stor Mater* 2020;33:298-308. DOI
  162. Li W, Wang F, Liu Y, et al. General strategy to synthesize uniform mesoporous TiO<sub>2</sub>/graphene/mesoporous TiO<sub>2</sub> sandwich-like nanosheets for highly reversible lithium storage. *Nano Lett* 2015;15:2186-93. DOI
  163. Chen M, Lu Q, Jiang S, et al. MnO<sub>2</sub> nanosheets grown on the internal/external surface of N-doped hollow porous carbon nanospheres as the sulfur host of advanced lithium-sulfur batteries. *Chem Eng J* 2018;335:831-42. DOI
  164. Zhang C, Park S, O'Brien SE, et al. Liquid exfoliation of interlayer spacing-tunable 2D vanadium oxide nanosheets: high capacity and rate handling Li-ion battery cathodes. *Nano Energy* 2017;39:151-61. DOI
  165. Mei J, Liao T, Kou L, Sun Z. Two-dimensional metal oxide nanomaterials for next-generation rechargeable batteries. *Adv Mater* 2017;29:1700176. DOI
  166. Kou H, Li X, Shan H, Fan L, Yan B, Li D. An optimized Al<sub>2</sub>O<sub>3</sub> layer for enhancing the anode performance of NiCo<sub>2</sub>O<sub>4</sub> nanosheets for sodium-ion batteries. *J Mater Chem A* 2017;5:17881-8. DOI
  167. Ramkumar R, Minakshi M. Fabrication of ultrathin CoMoO<sub>4</sub> nanosheets modified with chitosan and their improved performance in energy storage device. *Dalton Trans* 2015;44:6158-68. DOI PubMed
  168. Zhu Y, Cao C, Zhang J, Xu X. Two-dimensional ultrathin ZnCo<sub>2</sub>O<sub>4</sub> nanosheets: general formation and lithium storage application. *J Mater Chem A* 2015;3:9556-64. DOI
  169. Zhu J, Song D, Pu T, et al. Two-dimensional porous ZnCo<sub>2</sub>O<sub>4</sub> thin sheets assembled by 3D nanoflake array with enhanced

- performance for aqueous asymmetric supercapacitor. *Chem Eng J* 2018;336:679-89. DOI
170. Yadav AA, Chavan U. Electrochemical supercapacitive performance of spray deposited  $\text{Co}_3\text{O}_4$  thin film nanostructures. *Electrochim Acta* 2017;232:370-6. DOI
171. Jiang Y, Chen L, Zhang H, et al. Two-dimensional  $\text{Co}_3\text{O}_4$  thin sheets assembled by 3D interconnected nanoflake array framework structures with enhanced supercapacitor performance derived from coordination complexes. *Chem Eng J* 2016;292:1-12. DOI
172. Lu Z, Ding J, Lin X, et al. Low-temperature synthesis of two-dimensional nanostructured  $\text{Co}_3\text{O}_4$  and improved electrochemical properties for lithium-ion batteries. *Powder Technol* 2017;309:22-30. DOI
173. Sennu P, Madhavi S, Aravindan V, Lee YS.  $\text{Co}_3\text{O}_4$  nanosheets as battery-type electrode for high-energy Li-ion capacitors: a sustained Li-storage via conversion pathway. *ACS Nano* 2020;14:10648-54. DOI PubMed
174. Li S, Zhang J, Chao H, et al. High energy density lithium-ion capacitor enabled by nitrogen-doped amorphous carbon linked hierarchically porous  $\text{Co}_3\text{O}_4$  nanofibers anode and porous carbon polyhedron cathode. *J Alloy Compd* 2022;918:165726. DOI
175. Xu Z, Yao K, Fu H, et al. Constructing  $\text{MoO}_2$  porous architectures using graphene oxide flexible supports for lithium ion battery anodes. *Glob Chall* 2017;1:1700050. DOI PubMed PMC
176. Duan L, Li X. Lithiated  $\text{Mo}_4\text{O}_{11}$  to improve excellent cycle stability of  $\text{MoO}_2$  nanoparticles for lithium-ion battery. *Synthetic Met* 2021;272:116672. DOI
177. Zhao X, Wang HE, Cao J, Cai W, Sui J. Amorphous/crystalline hybrid  $\text{MoO}_2$  nanosheets for high-energy lithium-ion capacitors. *Chem Commun* 2017;53:10723-6. DOI
178. Liu Y, Ding C, Xie P, et al. Surface-reconstructed formation of hierarchical  $\text{TiO}_2$  mesoporous nanosheets with fast lithium-storage capability. *Mater Chem Front* 2021;5:3216-25. DOI
179. Liu C, He Z, Niu J, et al. Two-dimensional  $\text{SnO}_2$  anchored biomass-derived carbon nanosheet anode for high-performance Li-ion capacitors. *RSC Adv* 2021;11:10018-26. DOI PubMed PMC
180. Wang D, Zhang G, Shan Z, Zhang T, Tian J. Hierarchically micro-/nanostructured  $\text{TiO}_2$ /micron carbon fibers composites for long-life and fast-charging lithium-ion batteries. *ChemElectroChem* 2018;5:540-5. DOI
181. Ma Y. Sol-gel synthesis of  $\text{ZnO}/\text{TiO}_2$  core-shell nanocomposites and their structural and electrochemical characterization as anode for lithium ion battery. *Int J Electrochem Sci* 2020;15:12559-68. DOI
182. Ji Y, Lu X, Luo F, Zhang W, Tian Q, Sui Z. Improved  $\text{SnO}_2/\text{C}$  composite anode enabled by well-designed heterogeneous nanospheres decoration. *Chem Phys Lett* 2021;763:138242. DOI
183. Wu M, Zheng W, Hu X, et al. Exploring 2D energy storage materials: advances in structure, synthesis, optimization strategies, and applications for monovalent and multivalent metal-ion hybrid capacitors. *Small* 2022;18:e2205101. DOI
184. Wang H, Feng H, Li J. Graphene and graphene-like layered transition metal dichalcogenides in energy conversion and storage. *Small* 2014;10:2165-81. DOI
185. Wang R, Wang S, Jin D, et al. Engineering layer structure of  $\text{MoS}_2$ -graphene composites with robust and fast lithium storage for high-performance Li-ion capacitors. *Energy Stor Mater* 2017;9:195-205. DOI
186. Wang L, Zhang X, Li C, et al. Recent advances in transition metal chalcogenides for lithium-ion capacitors. *Rare Met* 2022;41:2971-84. DOI
187. Chen K, Balla I, Luu NS, Hersam MC. Emerging opportunities for two-dimensional materials in lithium-ion batteries. *ACS Energy Lett* 2017;2:2026-34. DOI
188. Zhao Z, Chao Y, Wang F, et al. Intimately coupled  $\text{WS}_2$  nanosheets in hierarchical hollow carbon nanospheres as the high-performance anode material for lithium-ion storage. *Rare Met* 2022;41:1245-54. DOI
189. Chaturvedi A, Hu P, Aravindan V, Kloc C, Madhavi S. Unveiling two-dimensional  $\text{TiS}_2$  as an insertion host for the construction of high energy Li-ion capacitors. *J Mater Chem A* 2017;5:9177-81. DOI
190. Liu S, Jia K, Yang J, et al. Encapsulating flower-like  $\text{MoS}_2$  nanosheets into interlayer of nitrogen-doped graphene for high-performance lithium-ion storage. *Chem Eng J* 2023;475:146181. DOI
191. Zheng L, Xing T, Ouyang Y, Wang Y, Wang X. Core-shell structured  $\text{MoS}_2$ @Mesoporous hollow carbon spheres nanocomposite for supercapacitors applications with enhanced capacitance and energy density. *Electrochim Acta* 2019;298:630-9. DOI
192. Jiang J, Zhang Y, An Y, et al. Engineering ultrathin  $\text{MoS}_2$  nanosheets anchored on N-doped carbon microspheres with pseudocapacitive properties for high-performance lithium-ion capacitors. *Small Methods* 2019;3:1900081. DOI
193. Ju J, Zhang L, Shi H, Li Z, Kang W, Cheng B. Three-dimensional porous carbon nanofiber loading  $\text{MoS}_2$  nanoflake-flowerballs as a high-performance anode material for Li-ion capacitor. *Appl Surf Sci* 2019;484:392-402. DOI
194. Yi S, Wang L, Zhang X, et al. Recent advances in MXene-based nanocomposites for supercapacitors. *Nanotechnology* 2023;34:432001. DOI
195. Yu P, Cao G, Yi S, et al. Binder-free 2D titanium carbide (MXene)/carbon nanotube composites for high-performance lithium-ion capacitors. *Nanoscale* 2018;10:5906-13. DOI
196. Brady A, Liang K, Vuong VQ, et al. Pre-sodiated  $\text{Ti}_3\text{C}_2\text{T}_x$  MXene structure and behavior as electrode for sodium-ion capacitors. *ACS Nano* 2021;15:2994-3003. DOI
197. Wang L, Zhang X, Li C, et al. Cation-deficient T-Nb $_2\text{O}_5$ /graphene Hybrids synthesized via chemical oxidative etching of MXene for advanced lithium-ion capacitors. *Chem Eng J* 2023;468:143507. DOI
198. Huang J, Lu X, Sun T, et al. Boosting high-voltage dynamics towards high-energy-density lithium-ion capacitors. *Energy Environ Mater* 2023;6:e12505. DOI

199. Naguib M, Come J, Dyatkin B, et al. MXene: a promising transition metal carbide anode for lithium-ion batteries. *Electrochem Commun* 2012;16:61-4. [DOI](#)
200. Come J, Naguib M, Rozier P, et al. A non-aqueous asymmetric cell with a  $\text{Ti}_2\text{C}$ -based two-dimensional negative electrode. *J Electrochem Soc* 2012;159:A1368-73. [DOI](#)
201. Guo Z, Wang Z, Wang D, Gao Y, Liu J. A free-standing VN/MXene composite anode for high-performance Li-ion hybrid capacitors. *RSC Adv* 2022;12:13653-9. [DOI](#) [PubMed](#) [PMC](#)